Development of the Mars microbeam Raman spectrometer (MMRS)

Alian Wang,[1] Larry A. Haskin,[1] Arthur L. Lane,[2] Thomas J. Wdowiak,[4]
Steven W. Squyres,[5] Robert J. Wilson,[3] Larry E. Hovland,[3] Ken S. Manatt,[2]
Nasrat Raouf,[3] and Christopher D. Smith[6]

Received 6 March 2002; revised 18 June 2002; accepted 3 July 2002; published 30 January 2003.

[1] Raman spectroscopy is a powerful tool for mineral characterization and for detection of water and organic and inorganic forms of carbon. The Mars microbeam Raman spectrometer (MMRS) is designed for close-up analysis of rocks and soils in planetary surface exploration. The MMRS consists of a probe (in a flight unit to be deployed by a robotic arm) and a spectrograph, laser source, and electronics (in a flight unit to reside on a rover or lander). The Raman probe has a scanning optical bench that enables a 1-cm linear traverse across a target rock or soil, both on target materials as encountered and on fresh surfaces of rocks exposed by abrasion or coring. From these spectra, one can identify major, minor, and trace minerals, obtain their approximate relative proportions, and determine chemical features (e.g., Mg/Fe ratio) and rock textural features (e.g., mineral clusters, amygdular fill, and veins). One can also detect and identify organic species, graphitic carbon, and water-bearing phases. Extensive performance tests have been done on a brassboard model of the MMRS using a variety of geological materials (minerals, rocks, Martian meteorites, etc.). These tests show that a Raman spectrometer can be built that is suitably miniaturized, sufficiently robust, and low enough in power usage to serve as an on-surface planetary instrument, yet the spectrometer can retain high detection sensitivity and yield near laboratory quality spectra over a broad wavelength range. These features are essential to provide definitive mineralogy in a planetary exploration. *INDEX TERMS:* 3672 Mineralogy and Petrology: Planetary mineralogy and petrology (5410); 3694 Mineralogy and Petrology: Instruments and techniques; 3994 Mineral Physics: Instruments and techniques; 5494 Planetology: Solid Surface Planets: Instruments and techniques; *KEYWORDS:* Raman spectroscopy, Mars in-situ mineralogy, Planetary on-surface mineral identification, Water on Mars, Miniaturized Raman spectrometer, Mars Microbeam Raman Spectrometer

Citation: Wang, A., L. A. Haskin, A. L. Lane, T. J. Wdowiak, S. W. Squyres, R. J. Wilson, L. E. Hovland, K. S. Manatt, N. Raouf, and C. D. Smith, Development of the Mars microbeam Raman spectrometer (MMRS), *J. Geophys. Res.*, *108*(E1), 5005, doi:10.1029/2002JE001902, 2003.

1. Introduction

[2] Exploration of Mars for the near future will emphasize themes of "life, water, and environment" [*EPO-NASA*, 1995]. Successful pursuit of these themes can benefit from definitive, detailed knowledge of the mineralogy of Martian surface materials and a search for water and organic carbon. "Definitive" mineralogy means unambiguous identification of minerals, determination of proportions of different minerals in rocks or soils, and determination of chemical compositions of minerals. From detailed mineralogy, we can discover past Martian environmental conditions. Such conditions may include subaerial alteration of rock surfaces, fluvial and marine alteration and deposition, and hydrothermal alteration and deposition, as well as the planet's early igneous chemical differentiation. By combining information about past environments with information about Martian organic carbon and inorganic reduced carbon, we can speculate rationally on the possible development of life on Mars and better assess the possibility of retention of fossils, particularly microbial ones.

[3] The most definitive studies of mineralogy of Martian materials, including evidence regarding the issue of life, will take place in laboratories on Earth, once sample-return missions take place. Meanwhile, in situ analysis of mineralogy using visible, IR, and Mössbauer spectroscopy is planned for upcoming missions (instruments similar to those described by *Squyres et al.* [1999], *Christensen et al.* [2001], and *Rieder et al.* [1997]). In this paper, we

[1]Department of Earth and Planetary Sciences and McDonnell Center for the Space Sciences, Washington University, St. Louis, Missouri, USA.
[2]Earth and Space Sciences Division, Jet Propulsion Laboratory, Pasadena, California, USA.
[3]Observational Systems Division, Jet Propulsion Laboratory, Pasadena, California, USA.
[4]Department of Physics, University of Alabama at Birmingham, Birmingham, Alabama, USA.
[5]Center for Radiophysics and Space Physics, Cornell University, Ithaca, New York, USA.
[6]Engineering Services, Swales Aerospace Corp., Pasadena, California, USA.

0148-0227/03/2002JE001902$09.00

present an alternative method for on-surface determination of mineralogy and to assist in sample selection: microbeam Raman spectroscopy [*Wang et al.*, 1995]. This method is rapid and sensitive. It provides information about chemical bonding and crystal structure, and thus enables direct identification of oxyanionic minerals (SiO_4^{4-}, CO_3^{2-}, SO_4^{2-}, PO_4^{3-}, etc.), oxide and sulfide minerals (FeOOH, Fe_2O_3, Fe_3O_4, FeS, FeS_2, TiO_2, etc.), water and water-bearing minerals (ice, $CaSO_4 \cdot 2H_2O$, micas, clay minerals, clathrates, etc.) and organic and inorganic carbon [*Wang et al.*, 1994]. It can provide information on rock texture, and it can determine cation ratios in many minerals.

[4] Our implementation of Raman spectroscopy includes scanning across the target surface with a microbeam, which enables statistical estimates of relative abundance for major minerals and detection of minor and trace minerals. The purpose of this paper is to present the performance of a Raman microanalytical instrument, the Mars microbeam Raman spectrometer (MMRS), which has been designed as a prototype instrument for a landed Mars mission. The prototype instrument shows that a space flight version of the instrument can be simple, robust, low mass, small volume, conservative of power, and able to work in the harsh environments encountered by flight instruments. The prototype instrument has the sensitivity and spectral range and quality that approach those of a modern laboratory Raman instrument. It can scan unmodified surfaces of rocks and soils as encountered, without sample preparation, as well as examine abraded rock surfaces and cores. Here, we report the characteristics and testing of the current model (''brassboard'') of this miniaturized Raman system to indicate the potential of this technique. The brassboard is based on a less sophisticated ''breadboard'' instrument described previously [*Wang et al.*, 1998a].

2. Characteristics and Development of the MMRS

[5] The MMRS has a probe, in the space flight version to be deployed by the robotic arm of a rover or lander; and a spectrograph, a laser, and electronics (including a microprocessor) to be mounted on or in the body of the rover or lander. Electrical cables will extend from the rover to the probe for power and monitoring, and optical fibers will connect the probe and the spectrograph for signal transfer.

[6] The MMRS brassboard, described here, tests these configurations. The brassboard probe dimensions are $\sim$5.7 $\times$ 7.0 $\times$ 7.5 cm (Figure 1a), and the brassboard spectrograph dimensions are $\sim$11.5 $\times$ 14.0 $\times$ 5.9 cm (Figure 1b); the flight MMRS probe and spectrograph are expected to be the same size or slightly smaller. A schematic diagram of the system is shown in Figure 2. For the MMRS brassboard described here, it was premature to produce the electronic boards in miniaturized form, because the nature of the rover or lander accommodations are not yet known, but they can fit within dimensions of 20 $\times$ 15 $\times$ 8 cm, based on our preliminary engineering design. The laser and its power supply have also not been miniaturized, but will have dimensions $\sim$3 $\times$ 3 $\times$ 5 cm, based on dimensions of commercial devices. The total mass of the MMRS system is $\sim$2.5 kg, of which the mass of the probe is just under 200 g. Operationally, the MMRS probe will be positioned against the target at a time convenient to the deploying host system, and it will collect spectra during the Mars early night. A set of 50–200 Raman spectra will be taken from the target during a 1–4-hour period. Total energy usage is estimated to be $\sim$35 Wh for a set of 100 spectra.

[7] Our Raman system was designed to satisfy two extremes. On the one hand, like any flight instrument, it needs to be simple, robust, low mass, economical of power, and able to work in a harsh environment. It must be stable against the mechanical stresses of launch, landing, rover travel, and arm deployment. The probe must function properly under harsh environmental conditions that include daily temperature cycling over a range of $\sim$100°C, nighttime operation at low temperature (as low as $-$60°C), low atmospheric pressure, and irradiation by cosmic rays. On the other hand, to achieve the goals of mineral characterization, an on-surface Raman system should cover a broad spectral region and have adequate spectral resolution and detection sensitivity. Our system covers the range 200–1800 cm^{-1} for characterization of minerals and graphitic carbon, and 2500–4000 cm^{-1} for detection of organic functional groups and water. Our instrument design called for a spectral resolution of $\sim$7 cm^{-1} to give a wave number precision of $\leq$2 cm^{-1} for peak positions; this was nearly achieved, and that resolution is shown to be adequate for our measurements. The probe delivers $\sim$10 mW of laser power to the target. To achieve a high tolerance of the relief intrinsic to unprepared, rough sample surfaces (rock or soils) without an autofocus mechanism, the probe has a large depth-of-sampling field. To obtain a line of 100 spectra along a 1.2-cm traverse of the target surface, the probe uses a simple line-scan mechanism. Combining a microbeam with a line-scanning traverse capability increases the probability of finding minor minerals and weak Raman scattering phases because the spectrum obtained at most spots will be of only one or two minerals. The overall result of such a line scan is thus the identification of major minerals, minor minerals, and determination of rock texture, rough mineral proportions, and mineral chemistry [*Haskin et al.*, 1997]. Below, we discuss some properties of the current MMRS brassboard. Then, we describe its performance on several types of targets.

2.1. Raman Spectroscopy

[8] In Raman spectroscopy, monochromatic light (λ_0) from a source is scattered inelastically from the target material, for example, a mineral [*Long*, 1977]. The spectrometer rejects reflected light from the source and Rayleigh-scattered light of that same wavelength (λ_0), and it analyzes the longer wavelengths of the Raman-scattered light (Stokes lines, $\lambda_0 + \Delta\lambda$). The difference in wavelength between the source light and the scattered light corresponds to transition energies in the material that produced the scattering. This difference in wavelength, $\Delta\lambda$, normally given in units of wave number, cm^{-1}, is called the ''Raman shift.'' For example, inelastic scattering from the silicate mineral olivine gives Raman-scattered light of several principal wavelengths, and those wavelengths are characteristic of olivine. The transitions that give rise to these main peaks are Si-O vibrational motions, transitions whose energies correspond to those of midinfrared and far-infrared

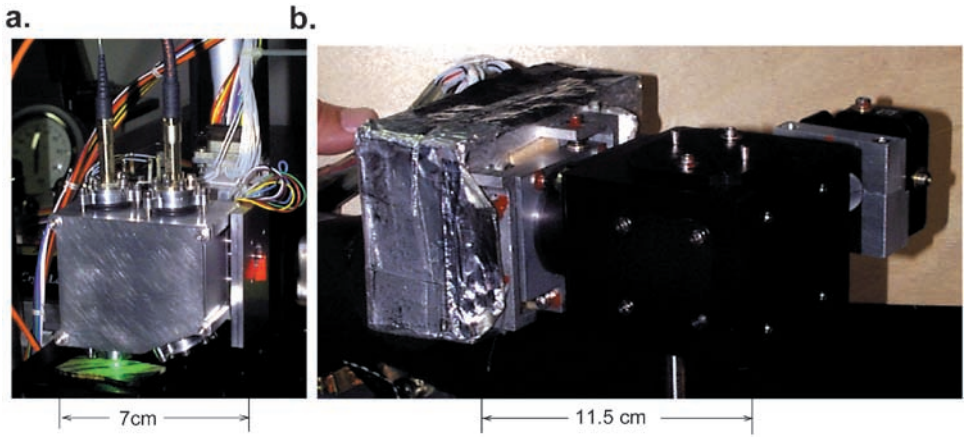

Figure 1. (a) The probe of the MMRS brassboard suspended above a small laboratory jack on which the sample rests. Although the laser beam is narrow (~28 μm) at the sample, multiple reflections give the pool of green light seen in the figure. (b) The MMRS spectrograph (black) is attached to a laboratory cooling box (covered with aluminum foil) to chill the CCD; on Mars, such a cooler will not be needed.

photons. For many minerals, a plethora of minor peaks is also produced. A technological advantage of Raman spectroscopy is that it provides information similar to that obtained by midinfrared and far-infrared spectroscopy, but the spectra can be obtained in the visible spectral region where Raman spectroscopy is efficient. Also, lasers and detection systems in the visible region of the spectrum are well understood and have space flight heritage because most optical and electro-optical components have their best performances there and have a long history of successful fabrication.

2.2. Selection of Excitation Wavelength and Lasers

[9] Because the Raman effect is weak, a laser excitation source is required for practical for use. Shorter excitation wavelengths are the most effective for a given laser power because of the $1/\lambda^4$ dependence of Raman scattering intensity. For an on-surface planetary application, small volume

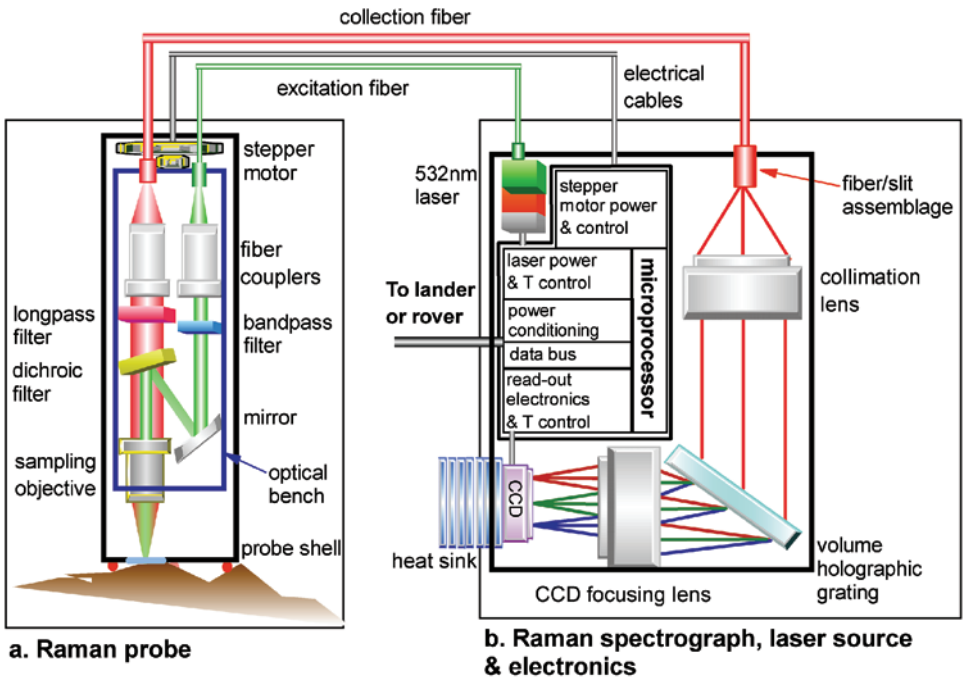

Figure 2. A schematic diagram of the probe, spectrograph, and ancillary units as they would be distributed between a mechanical arm and the rover or lander body in a spacecraft application. The diagram shows the optical components, their relative positions, and the light path. Power comes to the system from the host rover or lander and is conditioned by the instrument. Data for the set of spectra are sent from the microprocessor to the host for transmission to Earth. The probe shell is shown pressed against the uneven surface of a rock. The scanning motion of the optical bench within the probe shell is perpendicular to the page.

and low power are important. For mineralogical work, relative freedom from photoluminescent interference in the fundamental vibrational regions of oxyanionic minerals, oxide and sulfide minerals, and H_2O and OH is important. After experimental tests with lasers of a range of wavelengths, we elected to use a 532 nm (green) laser for the MMRS. Small, mechanically robust, relatively power-efficient lasers of this wavelength, (diode pumped, frequency-doubled YVO_4/Nd + KTP devices) have recently become commercially available (e.g., CrystaLaser, MIT Lincoln Laboratory, NanoLaser, and Synoptics).

2.3. Probe Design

[10] In the brassboard unit, called BB1d, the excitation laser beam (wavelength λ_0) reaches the probe via an optical fiber (see Figure 2). A narrow band-pass filter within the probe removes the Raman signal produced within that fiber. A lens focuses the laser beam onto the sample and collects the backscattered radiation from the sample, which includes reflected laser light (wavelength λ_0), Rayleigh-scattered light (also λ_0), and Raman-scattered light. The probe filters out the reflected and Rayleigh-scattered radiation and directs the Raman signal to a second optical fiber that leads to the spectrograph.

[11] Compared with various laboratory and industrial Raman systems, the probe design of the MMRS is specialized in five principal ways. First, a probe design using an objective lens rather than a fiber-only probe design (e.g., single-fiber, fiber-bundle, or dual-fiber) [*Schoen et al.*, 1992; *Sharma et al.*, 1993; *Cooney et al.*, 1996a, 1996b] was chosen because of the limited amount of laser power that may be available for a rover- or lander-based Raman system. A coaxial light path of excitation and collection ensures maximum cone overlap and thus maximum collecting efficiency of the Raman-scattered light. This is achieved by using the same objective lens to condense the laser beam onto the sample and to collect the scattered Raman radiation from the sample.

[12] Second, a multimode optical fiber was chosen instead of single-mode optical fiber for transfer of the excitation laser beam to the probe. This choice was made to improve system robustness against mechanical vibration and to make use of the higher coupling efficiency of excitation laser power that a multimode fiber offers. On the negative side, use of the multimode fiber (diameter $\sim$50 μm) limits how small the laser beam can be at the sampling spot. An f/1.2 lens system tightens the beam only to $\sim$28 μm diameter at the focal plane. (We anticipate obtaining a smaller spot, $\sim$10 μm, for the flight model MMRS.)

[13] Third, the manner of deployment of the MMRS affects the probe design. Raman spectral measurements will be done on the rough surfaces of rocks and soils mainly as they are encountered (i.e., without any sample preparation). The mechanical arm of the rover will position the MMRS probe by pressing it against the target, thus fixing the average distance between the sampling (and condensing) objective and the target. For simplicity and ruggedness, no automatic focusing is used. Instead, the probe has an effective depth-of-sampling field of several millimeters to accommodate the surface roughness anticipated for most samples. This is achieved by using a sampling objective with a long working distance ($\sim$1 cm) and a low numerical aperture (NA $\sim$0.45). A multimode optical fiber (d $\sim$200 μm) is used to collect the Raman signal from the probe and to transfer it to the spectrograph. This fiber acts like an oversized iris at the back-imaging plane of the sampling objective, and this makes it possible to collect Raman signal from off-focus planes of the sample. This configuration gives an effective depth-of-sampling field that considerably exceeds the depth of focus of the objective as normally considered. This large effective depth-of-sampling field is an advantage in Raman measurements on the uneven sampling surfaces of rocks. The use of the low NA objective and coarse core fiber to obtain a large depth-of-sampling field is in contrast to the current trend toward confocal Raman systems [*Dhamelincourt and Barbillat*, 1997; for planetary on-surface application, see *Dickensheets et al.*, 2000].

[14] Fourth, we obtain approximate proportions of minerals in a rock by a procedure analogous to petrographic point counting [*Haskin et al.*, 1997]. Point counting is an accepted method for determining modal abundances of minerals, and by using a microbeam instrument in that manner we avoid the pitfalls of "unmixing" spectral signals from a large spot. The MMRS makes a linear traverse along the surface of the target, obtaining spectra at 100 sampling points. In an unaltered crystalline rock, the volume proportion of each mineral equals the fraction of the points along the traverse at which that mineral is encountered (subject to statistical considerations). To accommodate point counting, a stepper motor moves the optical bench within the shell of the probe along the surface of the target in increments of $\sim$12.3 μm or multiples of $\sim$12.3 μm across $\sim$1.2 cm of the target surface. A spectrum is taken at each step. The condensed laser beam activates only a small volume of the target, which usually contains only one or two mineral grains, so only their spectra are recorded. One of those grains may be a minor or trace mineral in the rock or soil, but it provides a major part of the Raman signal at that sampling point. This procedure increases the probability of detecting minor and trace minerals as well as weak Raman scattering minerals, whose signals would be lost in the background noise of the minor peaks of strong Raman scattering minerals if they were simultaneously excited by a broad excitation laser beam. Peak positions are key for mineral identification; peak intensities are not used for that purpose.

[15] Finally, we use dielectric band-pass, dichroic, and long-pass edge filters (Barr Associates, Inc.) in the optical train of the probe. These filters are particularly suitable for on-surface planetary applications because they have extremely low coefficients of thermal expansion ($\sim 10^{-5}$/K). Raman signal is produced within the optical fiber that transmits the laser beam to the probe. This Raman signal extends to >1000 cm^{-1} and has a maximum near 430 cm^{-1}. The band-pass filter attenuates this signal, for example, by a factor of 10^{-5} (OD > 5) at a Raman shift position of 105 cm^{-1}. The filter has >80% transmittance at the excitation laser wavelength (532 nm), so it does not significantly decrease the laser power to the sample. The dichroic filter serves as a front-surface mirror to direct the laser beam toward the sampling objective. This same filter, when acting in transmissive mode has an OD >4.5 at λ_0 (=532 nm) to reject much of the component of the backscattered radiation (Rayleigh-scattered or reflected laser

radiation) and a transmittance of 93 ± 4% starting from 543 nm (Raman shift of ~380 cm^{-1}). This provides efficient transfer of the Raman signal from the sample. A long-pass edge filter provides additional rejection of λ_0 with an OD level of 4.5 at 532 nm, and an even higher transmittance (95 ± 4%) for Raman signals. Overall, the current probe reaches ~41% effective transmission for the 532 nm excitation beam, and ~64% for on-focus Raman signal collected at a Raman shift of ~3000 cm^{-1} (~633 nm).

2.4. Spectrograph Design

[16] The MMRS spectrograph receives the Raman radiation gathered by the probe via an optical fiber (Figure 2). This radiation is collimated, dispersed, and imaged onto a CCD detector (Charge Coupled Device). The MMRS spectrograph has an axially transmissive optical train. The major optical component that makes this configuration possible is a volume holographic transmissive grating (Kaiser Optical System, Inc.) that is matched by two sets of on-axis lenses for high-quality imaging. An advantage of a totally transmissive optical train in a flight spectrograph is its lower sensitivity to the unavoidable misalignments in a miniaturized instrument and to mechanical vibrations that may occur during rover mobility operations. The angular displacement of a ray caused by a misalignment or a mechanical vibration passing along a transmissive optical path is only half as large as it would be on passing along a reflective optical path.

[17] Also, from the point of view of optical design, a transmissive, on-axis optical train has intrinsically low aberration. By using multicomponent lenses for collimating and focusing, almost complete correction of the major aberrations (spherical aberration, coma, and astigmatism) can be reached over a large wavelength range. This allows low f number optics with a large solid angle of acceptance to be used. The low f number optics also enable a high throughput for Raman photons. The low aberration results in high imaging quality and high spectral resolution. For an axially transmissive spectrograph, it is easy to approach diffraction limited imaging, so that spectral resolution may be limited mainly by the width of pixels rather than by the point spread function of the optics. In addition, the low level of scattering by a volume holographic grating results in a lower level of stray light than is normally achieved using reflective components. The volume holographic grating we use has groove densities of 2455 lines/mm (lower Raman shift region) and 2156 lines/mm (higher region) to provide high angular dispersion. Lenses with very short focal lengths can therefore be used to attain high spectral resolution, and this allows the spectrograph to be compact [*Battey et al.*, 1993; *Arns*, 1995].

[18] Any dispersive spectrograph involves a trade-off between spectral coverage and spectral resolution to match a detector of fixed length. A transmissive, dual-blaze HoloPlex™ grating can simultaneously disperse two separate spectral regions onto one CCD frame. Each spectral region can make full use of the 1088 channels (~20 pixels high) of the CCD detector. In this way, the spectrograph covers the spectral ranges (200–1800 and 2500–4000 cm^{-1}) required to achieve the detection of a wide variety of minerals and organic substances, yet with adequate spectral resolution (see below) to determine cation ratios of geologically important phases (e.g., pyroxenes, olivine, carbonates, and sulfates). With this dual-blaze grating, we achieve a spectrograph of low mass and volume with wide spectral coverage and high spectral resolution.

[19] In most high-performance laboratory Raman instruments, a fiber-slit assemblage is used. Raman radiation transported via an optical fiber can be either directly coupled to or imaged onto the slit to form a rectangular image of the collected Raman radiation. This image is registered on the CCD, and its width determines the spectral resolution. The throughput of such an assemblage depends on the core diameter of the optical fiber relative to the slit width, that width being established by the required spectral resolution. To achieve our desired spectral resolution, we require a 50 μm input aperture to our spectrograph. As described above, however, our collecting fiber is 200 μm in diameter, so we have chosen to sacrifice nearly 70% of the Raman signal in order to preserve resolution by using the 50 μm slit.

[20] In the MMRS brassboard, a three-element lens collimates the Raman beam received from the fiber-slit assemblage, and a four-element lens condenses the dispersed spectral images onto the CCD detector. This pair of multicomponent lenses is aberration corrected and provides a ~1:1 image of the slit onto the detector, which achieves the necessary spectral resolution.

[21] Because the MMRS operates in the visible spectral region, we use a silicon-based CCD camera as the detector. Specifically, we use a frame transfer, 1088 × 1088-pixel CCD chip with a pixel size of 12 × 12 μm (Phillips 1010) as the detector. An attractive feature of this CCD is its low dark current at relatively high temperatures (typically below 50 pA/cm^2 at 25°C). Our test results give a dark current as low as 10 pA/cm^2 at −21°C. Active cooling would thus be unnecessary for Raman measurements on Mars (e.g., 196–260 K at the 1-m mast of the Pathfinder lander at 19.33°N, 33.55°W). Only a simple heater would be needed to keep a stable working temperature during early nighttime operations on Mars. This device has its highest quantum efficiency in the green wavelength region (>25% between 532 and 580 nm), which is similar to the quantum efficiency of other CCDs used in commercial Raman spectrometers in this spectral region. Other features of this device include a readout speed of 30 frames/s, 200× vertical antiblooming, a choice of vertical or horizontal summing, a dynamic range of 5800:1, a full-well capacity of ~200,000 electrons, and a readout noise of ~5 electrons per pixel. The clocking and readout of the CCD are controlled by a microprocessor. For CCD readout, on-chip 1 × 4 vertical binning is currently being used, which yields a maximum of 2^{14} counts per binned stack. Adjustable summing over 6–7 binned stacks is done to obtain the spectrum from each image blaze. Processing of the Raman data is handled by a platform system processor using a LabView test program. All subsystems (laser, step motor, sensors, and heaters) and the interface with rover/or lander will be autonomously controlled by the MMRS electronics system.

2.5. Environmental Tolerances

[22] The MMRS must endure four different periods during a mission to Mars: liftoff from Earth (mainly, strong vibrations), cruise from Earth to Mars (long shelf life, cold temperatures, cosmic radiation), descent onto the Martian surface (deceleration, shock), and on-surface operations

(mainly cold or warm temperatures, temperature cycling, vibrations during rover movements, and cosmic radiation). Each period has somewhat different environmental hazards. Levels of accommodation for some environmental hazards are still being defined. Thermal stability requirements for the probe will differ from those for the spectrograph on the Martian surface because these two components are positioned at different locations. The probe will be mounted on the end of a robotic arm for in situ measurement and thus will directly experience the Mars temperature cycling. The probe must function during the early Martian night. Its required survival temperature range is −110 °C to +65°C, and its operating temperature will lie between −20°C and −70°C. The spectrograph can either be heated separately or be positioned inside of the warm electronic box (WEB) of the rover to mitigate the temperature extremes of the external environment. The survival temperature of the spectrograph is −55°C to +65°C, and it is for CCD cooling that the MMRS will operate during the Martian night.

[23] Several of the technologies required for a flight model MMRS have already been used or tested for space applications. These include mechanical mountings, dielectric filters, optical lenses, and stepper motors. The volume holographic grating has not yet flown in space, but is known to survive temperatures from −50°C to +80°C (Kaiser Optical Systems, Inc.). Our preliminary temperature cycling tests showed that a unit of same general physical structure and made of the same materials (a volume holographic notch filter) remained intact when cycled from −98°C to +105°C. The volume holographic grating, which will reside in the rover WEB, does not have to accommodate to that wide a temperature range, and no observable shift in its dispersion is anticipated (estimates of thermal expansion give <1 cm^{-1} shift per 60°K change in temperature for both spectral regions). Should a small shift occur, it would not greatly affect the Raman measurements, because a correction can be made on the basis of the internal calibration standard, which is measured with each spectral data set.

[24] Among the technologies involved with MMRS development, the biggest unknown until recently has been the mechanical survivability and the low temperature characteristics of the optical fibers. These fibers must be bent and twisted at low temperature during deployment of the instrument by a robotic arm, usually during the Martian day (T = +5 to −30°C). They must also follow the much smaller movement of the probe optical bench during point count traverses (∼1.2 cm, linear) during the much colder Martian night (T = −20 to −70°C). Extensive optical fiber performance tests at low temperatures have now been conducted, and detailed results will be published elsewhere (Keedy and Lane, personal communication, 2001). The first-order problem, protection of the fibers against accidental snags, whether during installation or operations, is avoided by the use of fibers sheathed in 1.5 mm diameter stainless steel capillaries. For testing, capillary-shrouded fibers in groups of four (one coarse fiber of 200 μm diameter, three finer fibers of 50 μm diameter) were curled into coils ∼19 mm in diameter. Each coil was then bent, twisted, or stretched continually for 10–20 hours in a cold bath at temperatures ranging from room temperature to −77°C. Variations in light throughput were negligible during both stretching–compressing and bending motions. Variations of ∼5 to 20% were observed during twisting motions, but light intensities returned to their original values as soon as the motion was stopped, whether or not the torque was still being applied and the capillary had relaxed. No fiber broke during these cold tests.

[25] The radiation tolerance requirement for MMRS is set as 2–3 krad over the lifetime of the mission. A test on a volume holographic filter (made of same materials and having the same physical structure as the volume holographic grating) conducted by Dr. R. Donchoe at Los Alamos National Laboratory showed no observable change in transmittance after 104 krad of ^{60}Co γ-ray radiation (Donchoe, personal communication, 1998).

[26] Tolerance requirements for mechanical vibration have not yet been set for the MMRS. The major concerns are vibrations during launch and acceleration, during separation of rocket stages, and on deceleration and landing, plus perhaps irregular jolts and vibrations during rover travel. We have selected Diamond AVIM optical fiber connectors (Rifocs Corp.) for their ruggedness for optical coupling of the fibers between the Raman probe and spectrograph. In addition to low light loss and a broad operating temperature range, this type of connector has high vibration and shock tolerance. In addition, both CW (continuous wave) and pulsed 532 nm laser systems of the type we anticipate using in the MMRS have passed 1G and 9G vibration tests (Crystalaser, Synoptics, personal communication, 2000). Minor optical misalignment caused by mechanical vibrations and shocks will be monitored by the use of the Raman peak intensity variation of the internal calibration target. This target (not yet selected) will be placed at the focal plane of the sampling objective when the optical bench is in its docking position in the Raman probe shell. The peak positions from this calibration target will also be used to correct for any change in Raman peak positions of measured samples resulting from temperature shift of optical elements and the laser or from environmentally produced alignment shifts.

3. Performance Tests of the MMRS Brassboard

[27] The MMRS system is designed to function under the conditions of the Mars surface. For the testing of the brassboard in our laboratory at room temperature, a stream of cold nitrogen gas was used to cool the CCD to −20°C. This provides the low dark current that the Mars evening temperature environment will automatically furnish. The CCD enclosure was purged with dry nitrogen to prevent water condensation from the laboratory atmosphere. Also, the Raman probe was suspended on an adjustable XYZ stage for positioning for measurements, analogous to the placement of the instrument by the robotic arm of a rover or a lander.

3.1. Basic Spectrometer Performance Tests

[28] Spectral coverage, spectral resolution, wavelength calibration, light throughput, overall spectral response, and line scanning are the essential aspects of spectroscopic performance that we have tested. The spectra of standard Hg and Ne lamps are shown in Figures 3a and 3b. The CCD wavelength scale was calibrated using a sixth-order polynomial regression for 11- and 15-point calibrations based on

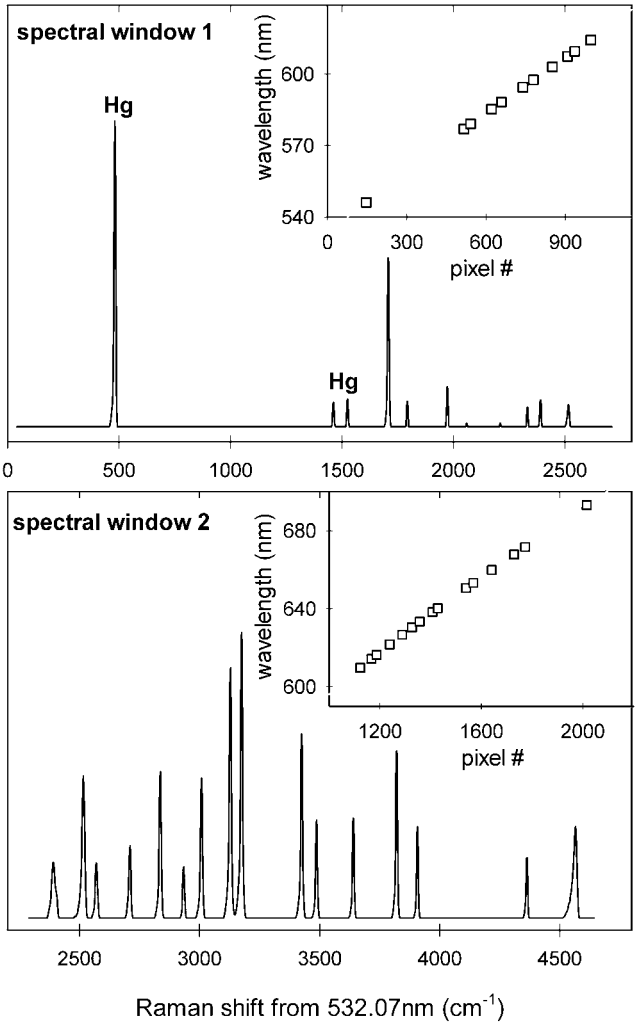

Figure 3. (a) A spectrum consisting of lines from Hg and Ne lamps is shown for spectral window 1, and the essentially linear relationship between wavelength and position on the CCD detector (as pixel number) is shown. (b) Similar diagrams are shown for spectral window 2.

Hg and Ne lines in both spectral windows. The error is <0.1 cm^{-1} across the entire length of each spectral window. A similar 12-point calibration based on Ar lines gives the same result for spectral window 1. The dispersions over the spectral range of interest are essentially linear (see the inserts in Figures 3a and 3b). On the CCD, the image of each blaze has a height of 24 pixels (~280 μm), and the vertical separation between the two blazes is 112 pixels. The first spectral window covers Raman shifts from 160 to 2645 cm^{-1}, corresponding to the spectral range of the fundamental vibrations of silicates, carbonates, phosphates, sulfates, and other oxyanionic compounds as well as most oxides, sulfides, and graphitic materials. The second spectral window covers Raman shifts from 2400 to 4600 cm^{-1}, corresponding to the spectral range of fundamental vibrations of C, N, and O with H in organic functional groups, and OH and water. The two spectral windows of the brassboard overlap in the 2400–2640 cm^{-1} region.

[29] Based on the spectral range of each blaze of the grating, we have calculated the wavelength spread per pixel and can predict the width of the slit image at the CCD camera. The 50 μm entrance slit width is just over four times larger than the 12-μm pixel width. The minimum image width on the CCD is the sum of the ideal slit image width plus the increase in width from diffraction, estimated to be ~3 μm, for a total of 51 μm, assuming an aberration-free system. In terms of CCD response, and noting that the edge of the image will likely be in the interior of a pixel rather than at the boundary between pixels, the image would usually be 5 pixels wide, or ~60 μm, but if the image fell in just the right location, it would extend across 6 pixels or 72 μm. The light is most intense toward the center of the image, giving rise to the peak shape shown in Figures 4a and 4b. Atomic emission lines of Hg, Ne, and Ar standard

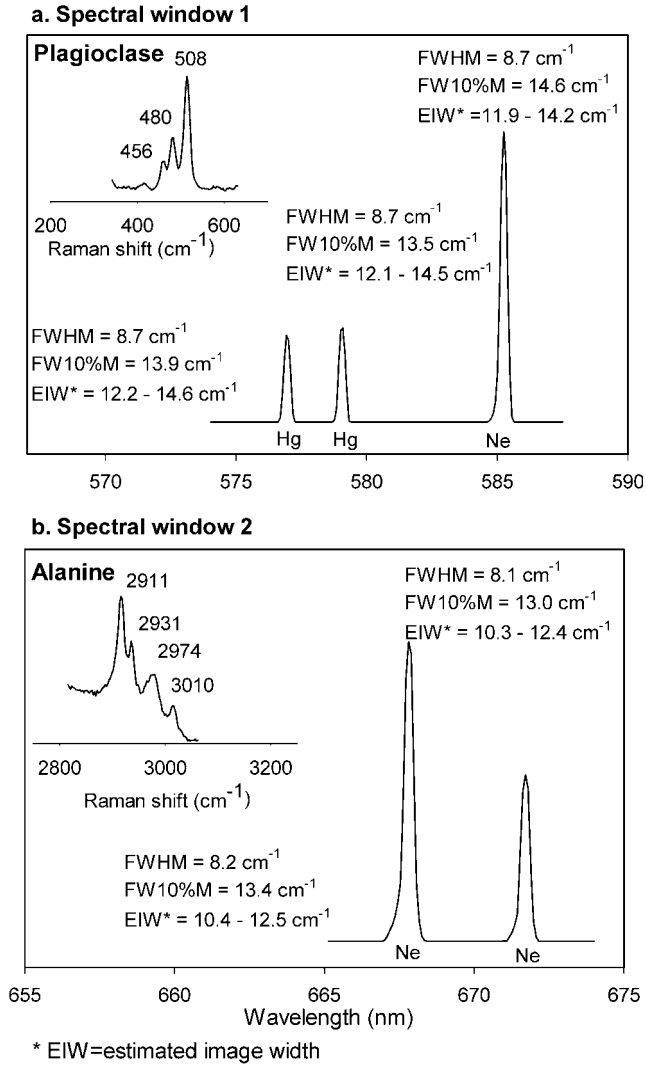

Figure 4. (a) The spectral resolution of window 1 is shown using two Hg lines and one Ne line and the observed widths are compared with estimated image widths (EIW) based on 1:1 imaging and diffraction limited resolution. The ability of the MMRS to resolve adequately the triplet of feldspar lines that fall in spectral window 1 is demonstrated. (b) The spectral resolution of window 2 is shown using two Ne lines and the ability to resolve CH vibrations of alanine is demonstrated.

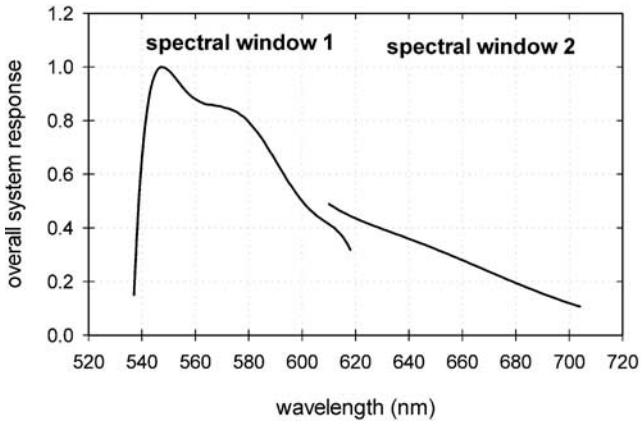

Figure 5. The relative overall system response for spectral windows 1 and 2 is shown. The main components giving rise to this response are the grating efficiency, the CCD response, and the transmittance of other optical elements, i.e., the filters, lens, and optical fibers, all of which are wavelength dependent. The sharp cutoff by the filters removes light of the laser wavelength in spectral window 1.

lamps were used, and we evaluated the imaging quality of the spectrograph by comparing the measured widths of their atomic lines with the estimated minimum image width if there are no aberrations. By curve fitting, we obtained the full width at 10% maximum (FW10%M), which we use as a rough measure of the peak width. Both the FW10%M and the more commonly used FWHM values are listed in Figures 4a and 4b, along with the estimated minimum width of the image (60 μm for 5 pixels or 72 μm of 6 pixels, and converted to wave number using the linear dispersions of the groove sets in the grating).

[30] The measured spectral line widths (FW10%M) of two Hg lines in spectral window 1 are 13.5 and 13.9 cm^{-1}. These values lie within the respective ranges of estimated image widths for 5 and 6 pixels of 12.2–14.6 and 12.1–14.5 cm^{-1} (Figure 4a, spectral window 1). The measured width of the neon line exceeds the 6-pixel width by ~0.4 cm^{-1}. The measured line widths of two Ne lines at longer wavelengths in spectral window 2 exceed the estimated values for 6 pixels by 0.6 and 0.9 cm^{-1}. That the lines are only ~2–5 μm broader than the estimated minimum image width (for zero aberration) indicates little aberration, well under 1-pixel width. Reasons for the additional broadening include deviations related to allowed tolerances in fabrication of the lenses (radius of curvature, thickness, position of the optical axis) and the grating (tilt of two sets of groves), and the mechanical mounting of the optical components (spacing, tilt, etc). The FWHM values for the Hg and Ne lines suggest that the spectral resolution of the current brassboard is 8–9 cm^{-1}. This enables location of Raman peaks to better than 2 cm^{-1} by curve fitting of spectral peaks. The two inserts in Figures 4a and 4b are Raman peaks obtained from mineral and organic samples. The spectral resolution of the MMRS brassboard enables the triplet in the fundamental vibrational modes of feldspar (Si-O framework) and the quadruplet stretching modes (C-H) of an amino acid (alanine) to be well resolved.

[31] The overall spectral response reflects the combined effects of the quantum efficiency of the CCD detector, the diffraction efficiency of the grating, and the transmittance and reflectance of the other optical components (filters, lens, optical fibers). A standard white light source of known spectrum has been measured using the MMRS brassboard; a sixth-order polynomial regression was used to fit the recorded spectrum in order to smooth out noise and modest filter ripple. The overall response curve was then obtained by correcting the smoothed spectrum to the emission curve of the white light source (Figure 5). The general shapes of the response curves for the two spectral windows demonstrate that the CCD and the grating in the MMRS brassboard are functioning as expected. The central high in spectral window 1 corresponds to the peak in grating efficiency for wavelengths in the middle of that spectral window. The sharp decrease in the response curve toward the λ_0 laser wavelength of 532 nm occurs because the dichroic and long-pass filters remove light of the laser wavelength from the collected light. The central high in spectral window 2 hardly perturbs the curve for that region because the strongest effect is the lower quantum efficiency of CCD in that region.

3.2. Tests on Geological Samples

[32] We have done three types of tests on geological samples. One set of tests was done on large individual mineral crystals and other substances with well prepared surfaces and under the most favorable experimental conditions. The purpose of this set was to compare the performance of the brassboard to that of our state-of-the-art laboratory HoloLab5000 Raman spectrometer (Kaiser Optical Systems, Inc.) and to exclude any interference from unfavorable sample conditions in making this comparison. The second set of tests was Raman point counting on rocks, where the mineral phases and other substances to be identified are embedded in rock matrices of different types and have a range of grain sizes. Most of the rock samples had flat, rough-sawn surfaces (a few original rough surfaces were also measured), but the measurements were moderately off-focus for most spots during the automatic linear scans. The purpose of this set was to understand how well the breadboard could be used to characterize rock samples under somewhat degraded experimental conditions. The third set of tests was done to determine the practical limit of the sampling depth of field for rough rock surfaces and for small grains.

3.2.1. Identification of a Wide Variety of Phases

[33] In consideration of actual and potential major geologic and mineralogic features of Mars, first-order tests were done on the major rock-forming minerals olivine, pyroxene, feldspar, quartz, and calcite. The same samples were measured using both the MMRS brassboard and the HoloLab5000, both using the same excitation wavelength (532 nm). The samples in this test all have flat surfaces, and measurements were done with the laser beams well focused on those surfaces so differences in surface geometry would be minimized. The same integration times were used for the measurements made on both systems, in order to get the most meaningful comparison of the S/N of the Raman spectra. Two sets of raw spectra obtained using the two systems are shown as Figures 6a and 6b. (Raw spectra are uncorrected for background or interferences such as photoluminescence.) To first order, both spectrometers give spectra of similar

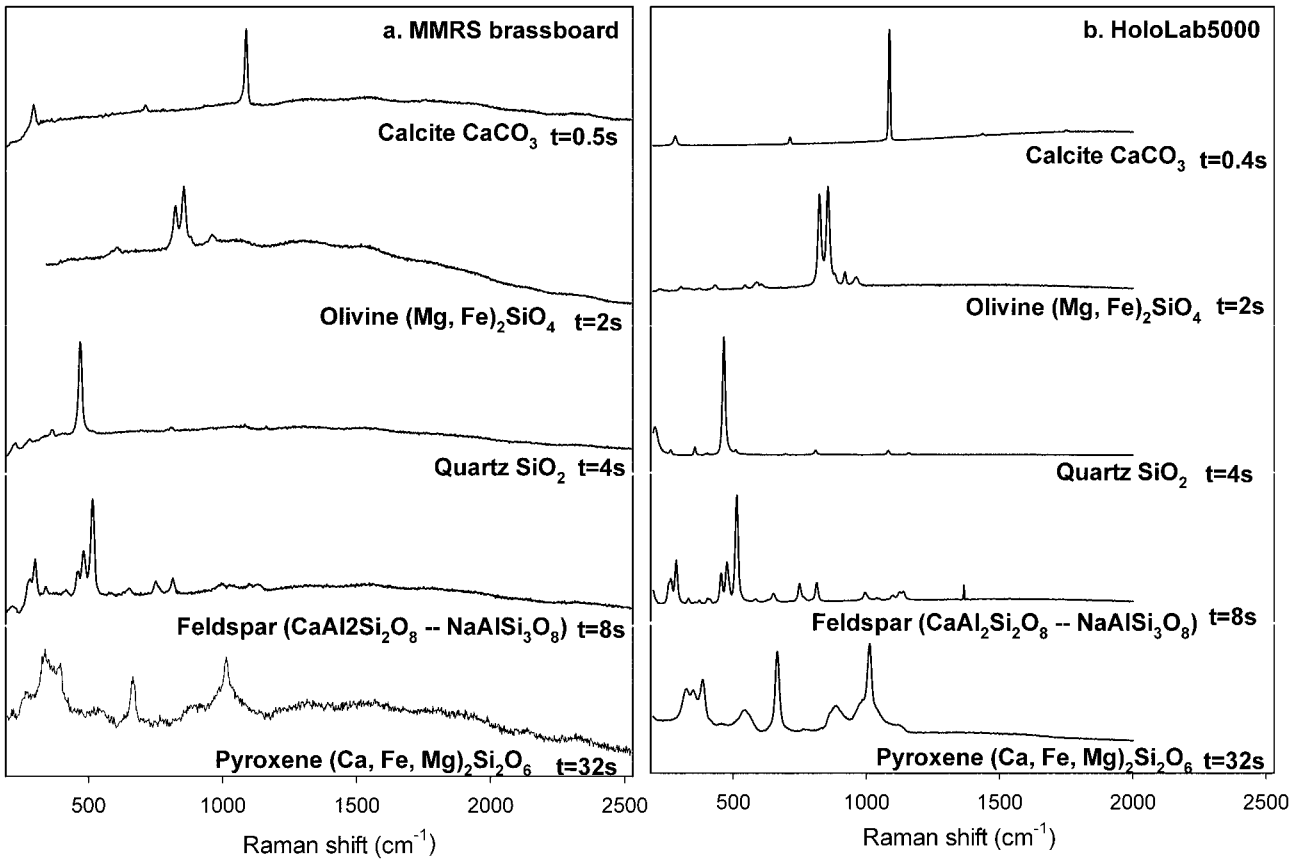

Figure 6. Raw spectra of large, single grains of several minerals taken on the MMRS brassboard (a) are compared to raw spectra of the same specimens taken on the HoloLab5000 (b). The integration times are the same (except for calcite). The laser power to the sample is 11 mW for the MMRS and 14 mW for the HoloLab5000, and the spectra have not been adjusted to compensate for this difference. Intensities are on an arbitrary scale and no quantitative comparison between the two systems is made; signal-to-noise ratio is the quantity of interest here.

quality, and identification of these mineral phases from the raw spectra is straightforward from either set.

[34] Phosphates, oxides, and sulfides occur as minor or trace phases in igneous rocks. Identification and characterization of these phases can be critical to understanding the history of a rock and the environment of its origin or alteration. Iron oxides and oxyhydroxides are abundant at the surface of Mars [e.g., *Madsen et al.*, 1999; *Hargraves et al.*, 2000; *Morris et al.*, 2000, 2001]. Iron oxides and iron sulfides are weaker Raman scatterers than silicate minerals and need longer integration times to get Raman spectra with acceptable S/N. They all have characteristic "fingerprint" spectra and are readily identified from their raw spectra [*Wang et al.*, 1998b, 2001a]. Examples obtained using MMRS brassboard are shown in Figure 7. In a linear traverse of 100 spectra on Mars, a preliminary spectrum will be taken at each traverse point. This preliminary spectrum will be processed to determine the necessary integration time for the spectrum to be taken at that spot. Thus, weak Raman scatterers such as Fe oxides can be given a minute or more of exposure to the laser beam to increase the chance of their detection, whereas strong scatterers (most major minerals) will be given only a few seconds per spectrum.

[35] Given the nature of the Mars atmosphere, the evidence of past volcanic activity, and reports suggesting the presence of sulfate and carbonate minerals in the remote sensing literature, we will want to be able to observe those minerals. (See the works of *Soderblom* [1992], *Bell* [1996], and *Bell et al.* [2000] for general discussions of remote sensing observations of CO_3^{2-} and SO_4^{2-} mineralogy on Mars. See the work of *Fonti et al.* [2001] for a recent discussion of CO_3^{2-} and references therein to previous observational work. Note that neither CO_3^{2-} or SO_4^{2-} minerals have so far been identified from orbit [*Christensen*, 2001].) Sulfate and carbonate minerals are mostly products of sedimentary and hydrothermal processes. Finding those minerals on Mars would be significant indication of recent or past aqueous chemical reactions. A set of raw spectra of carbonates and sulfates taken with the MMRS brassboard appears in Figures 8a and 8b. Oxyanionic minerals (carbonates, sulfates, silicates, and phosphates) are strong Raman scatterers. The characteristics of their major Raman peaks are controlled by the structural symmetry of anionic groups (CO_3^{2-}, SO_4^{2-}, SiO_4^{4-}, PO_4^{3-}, etc.), the strength and reduced mass of specific bonds (C-O, S-O, Si-O, P-O, etc.), and the overall structural arrangement of the anions within the

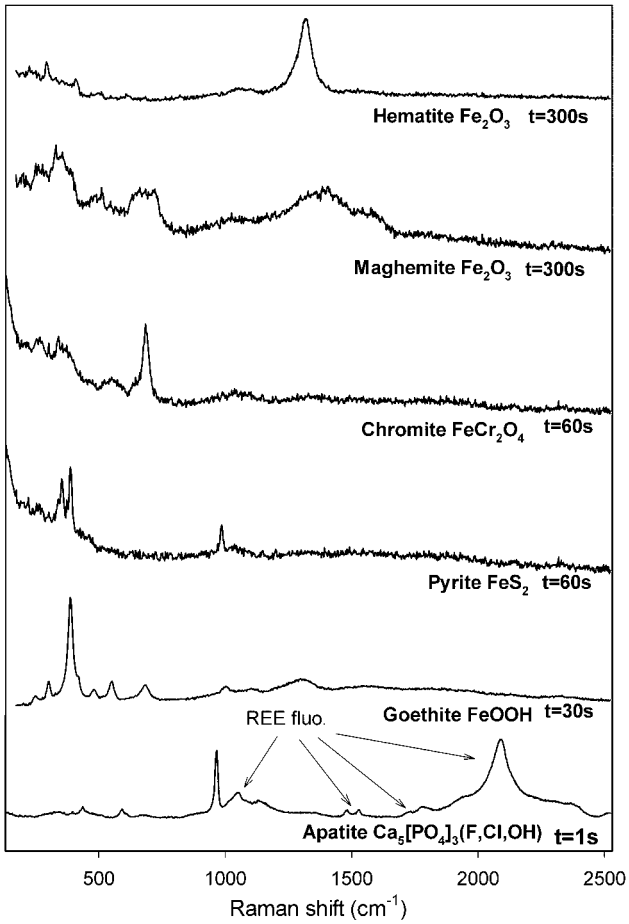

Figure 7. Raman spectra are shown for some Fe oxides, an Fe sulfide, and an apatite (a phosphate mineral). Note the relatively broad peaks of the hematite and maghemite and the fluorescence peaks from rare Earth elements in the apatite spectrum.

minerals. The major peaks of these minerals do not overlap each other, so a straightforward, first-order mineral classification can be achieved by direct inspection of the raw spectra even when the spectrum contains peaks from more than one mineral. The positions of Raman peaks and their relative intensities (i.e., the Raman spectral pattern) are affected to second order by the cations bonded to these oxyanionic groups. Therefore, detailed mineralogical characterization, such as cation ratios in carbonates or variation in the hydration state of sulfate, can be extracted by detailed analysis of Raman spectra. For example, the major, sharp peaks near $\sim$1085 and $\sim$990 cm^{-1} in Figure 8 are diagnostic of the CO_3^{2-} and SO_4^{2-} anionic groups, while the precise Raman shifts of those major and minor peaks indicate the identities or the proportions of the different cations [*Kuebler et al.*, 2001].

[36] Raman spectroscopy is a sensitive indicator of water and can identify the minerals in which it occurs. Spectral pattern and peak positions for OH vibrations vary with the degree of hydration and the local symmetry of the OH bonding in a mineral. Thus, an OH spectrum can appear as several sharp peaks indicative of specific, well defined OH bonding sites (e.g., in amphiboles), or broader "water" peaks with varying shapes affected by the degree of hydration (e.g., in phyllosilicates). Unambiguous identification of water-bearing minerals, both weak Raman scatterers (muscovite, chlorite, serpentine) and strong scatterers (epsomite, copper sulfate), is illustrated by the MMRS spectra in Figure 9. Note that the water signal is readily seen in both the weaker and stronger scatterers [*Wang et al.*, 2002].

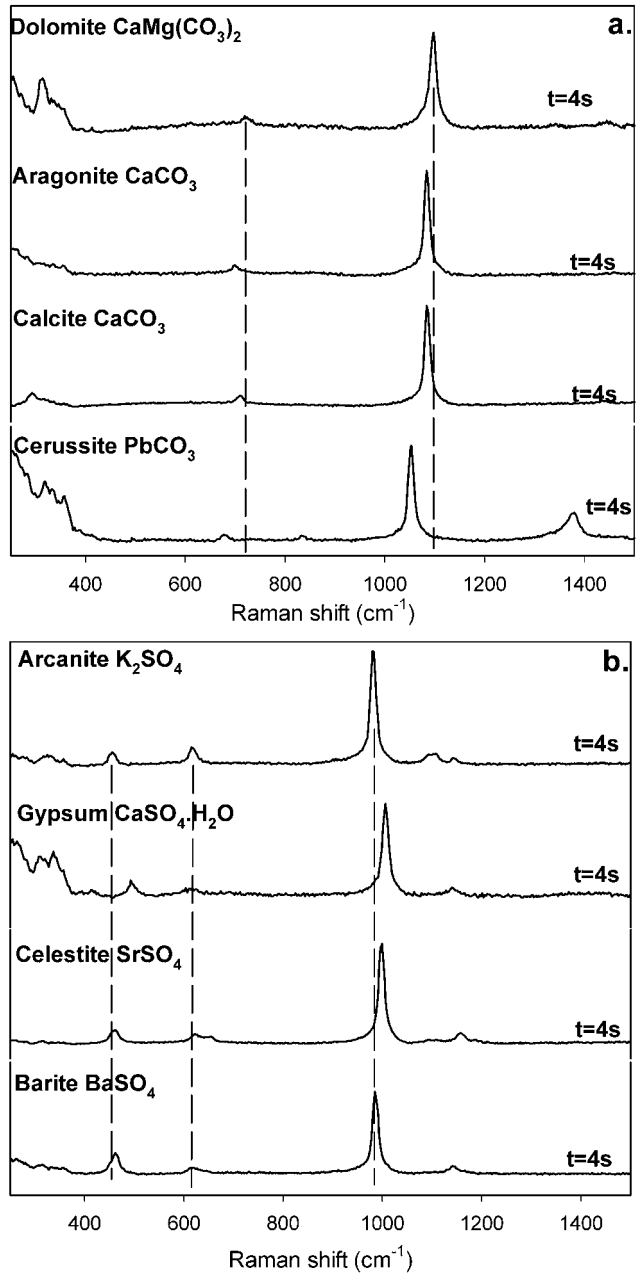

Figure 8. Raman spectra are shown for series of carbonate minerals (a) and sulfate minerals (b). Sulfates as generic groups can be easily distinguished from carbonates (and other oxyanionic minerals) because their principal peaks fall in slightly different regions of the spectrum. Individual sulfate minerals and carbonate minerals can be distinguished from each other because the exact positions of the peaks depend on which cation is present.

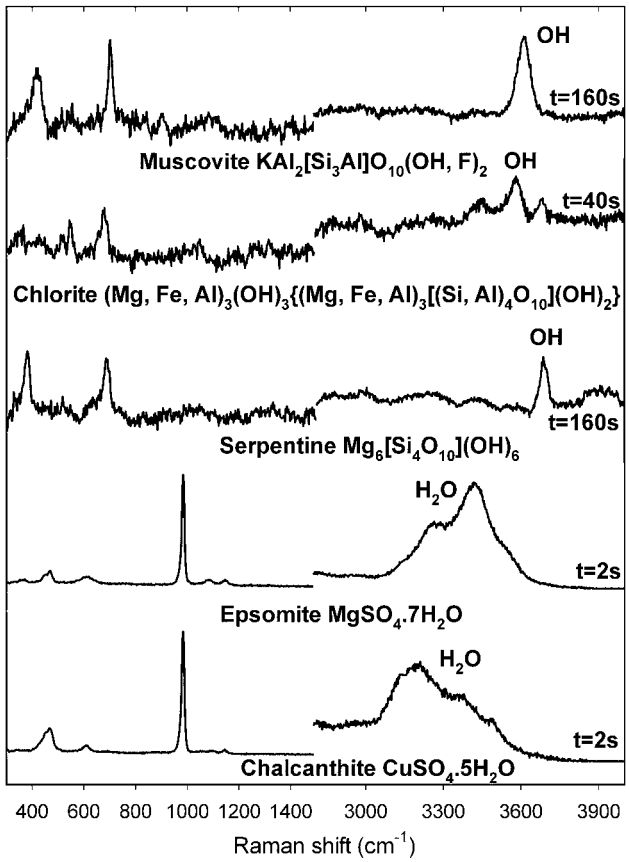

Figure 9. Spectra are shown of three phyllosilicate minerals and two hydrated sulfate minerals. Note the relatively sharp OH peaks in these phyllosilicates as opposed to the broader H_2O peaks in the sulfates. The broader peaks indicate that the positions of the H_2O in the crystal are less well defined.

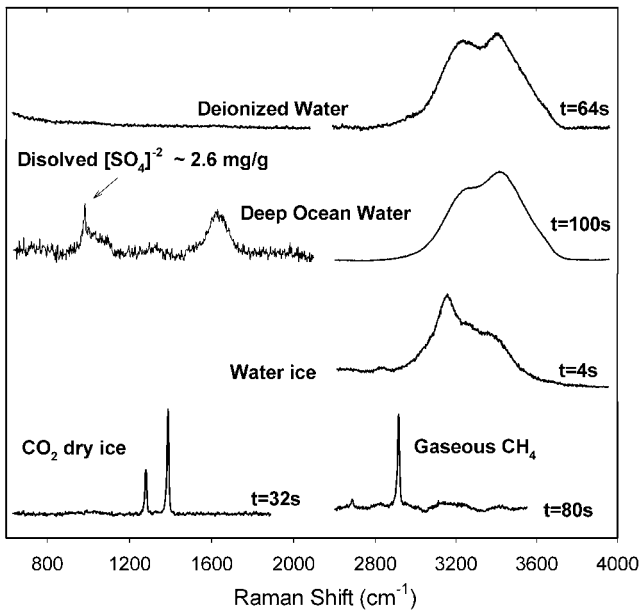

Figure 10. Spectra are shown for solid and liquid water, solid CO_2, and gaseous methane. Note the peak for SO_4^{2-} in the seawater ~980 cm^{-1}; the SO_4^{2-} concentration is ~2.6 mg/g.

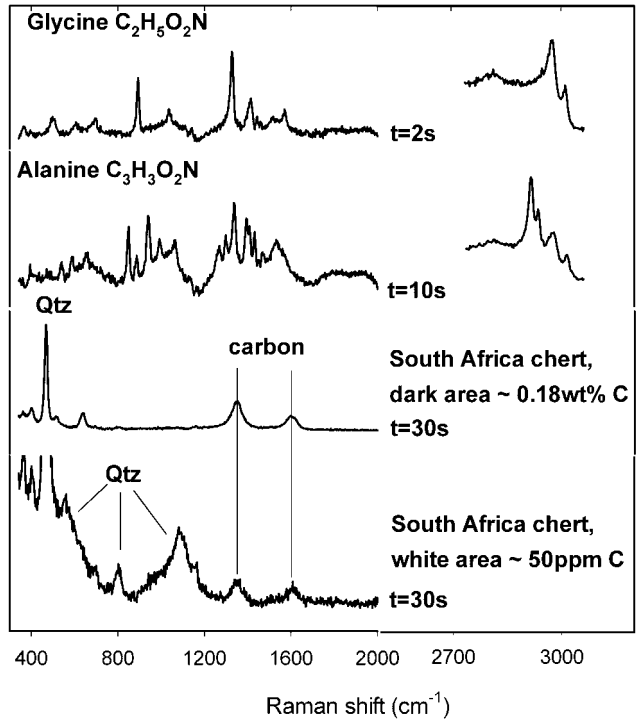

Figure 11. Spectra of organic chemicals (the amino acids glycine and alanine) and of disordered graphitic carbon believed to be the remains of ancient microorganisms. The spectra from the South African banded chert are from C-rich dark areas and C-poor white areas. The pair of C peaks indicates that the graphitic carbon is structurally disordered.

[37] The Raman peak shape and peak position of liquid water also vary with the type of dissolved ions. Differences in physical state (e.g., liquid water or water ice, gaseous CO_2, or dry ice) show obvious differences in spectral features (Figure 10). Note the major Raman peak of sulfate (~980 cm^{-1}) dissolved in seawater in which the sulfate concentration is only ~2.6 mg/g. Gaseous CO_2 has a characteristic double peak at 1286 and 1388 cm^{-1}, different from the peaks of dry ice (1277 cm^{-1}, and 1385 cm^{-1}) and also slightly different from those of CO_2–H_2O clathrate. Gaseous methane (CH_4) has a major peak at 2940 cm^{-1}; the CH_4–H_2O clathrate peak occurs at a different position (2905 cm^{-1}) [*Sum et al.*, 1997]. Water ice and CO_2–H_2O clathrate have been proposed as major subsurface carriers of H_2O and CO_2 on Mars [*Kargel et al.*, 2000; *Longhi*, 2000, 2001; *Komatsu et al.*, 2000].

[38] Any organic compounds found on Mars will be of interest. Compared to minerals, organic compounds are stronger Raman scatterers and can thus be detected at low concentrations. In addition, the positions of their major peaks and their spectral patterns are different from those of minerals. Distinguishing between organic and inorganic materials based on their Raman features is therefore straightforward [e.g., *Edwards et al.*, 1999; *Wynn-Williams and Edwards*, 2000]. The major vibrational modes of H bonded to O, C, and N give peaks in the upper spectral region (2500–4000 cm^{-1}). These peaks are extremely sharp, and strong multiplets occur. The general locations of these multiplets (CH ~2800–3100 cm^{-1}, NH ~3000–

Table 1. Point Counting Raman Measurement on Rock Samples

Rocks	Traverse number	Type of surface	Integration time (s)	Step size (μm)	Scan length (mm)	Number of spectra	Interpretable spectra (%)	% mineral detected
EETA79001, meteorite chip[a]	1	Original	64	123	1.0	8	100	pyroxene (87.2),
	2	Original	64	123	2.46	20	100	olivine (12.4),
	3	Original	32	246	12.3	50	96	phosphate (0.4)
	4	Original	32	246	11.3	46	98	
Ortenburg basalt	1	Flat sawn	64	123	2.5	20	95	pyroxene (15.9),
	2	Flat sawn	64	123	5.65	46	93	olivine (15.1) feldspar (69.1)
FRB basalt	1	Flat sawn	64	123	2.5	20	95	pyroxene (33.2),
	2	Flat sawn	64	123	6.15	50	98	feldspar (38.1), sphene (20.2), hematite (8.5)
Calc-silicate amphibolite	1	Flat sawn	32	61.5	1.2	20	95	feldspar,
	2	Flat sawn	32	123	2.5	20	100	amphibole,
	3	Flat sawn	32	615	7.3	12	75	epidote, quartz
AKB basalt (amygdule)	1	Flat sawn	4	123	2.46	20	100	calcite, zeolite
Missouri red granite	1	Original	16	123	1.3	11	100	feldspar, quartz
	2	Original	8	123	1.23	10	70	
	3	Flat sawn	8	615	12.3	20	100	
Mojave tufa 3256	1	Flat sawn	1	246	4.92	20	65	Calcite (100)
South Africa chert	1	Flat sawn	8	246	4.92	20	100	Graphite (100), quartz (100)
Manson impactite	1	Flat sawn	2	615	12.3	20	95	feldspar, quartz, calcite

[a] Maskelynite, a glass of feldspar composition, is also present but difficult to detect (see text).

3500 cm^{-1}, OH ~3400–3800 cm^{-1}) can be used to distinguish among them. The major peaks that arise from bonds between C, O, N, and S in organic compounds occur in the lower spectral region (200–1700 cm^{-1}). Spectra are shown of two simple amino acids, glycine and alanine (Figure 11), taken by using the MMRS brassboard. As organic materials, including those of biogenic origin, undergo metamorphism, they are processed into kerogen or similar materials. The Raman spectra of these degraded materials can range from complicated organic spectra, to mainly a photoluminescence background, to graphite. In some metamorphosed rocks, we observe a poorly ordered form of C showing a broad peak in the range for graphite (~1600 cm^{-1}) and a second broad peak at a lower Raman shift (~1360 cm^{-1}) [*Wopenka and Pasteris*, 1993]. We will refer to the materials giving such a double-peaked spectrum as "disordered graphitic C." We have observed disordered graphitic carbon presumed to come from ancient organisms in ancient cherts, for example [*Wang et al.*, 2001b; see also *Kudryavtsev et al.*, 2001]. This type of carbon might be the principal or only remaining evidence of ancient life on Mars. (The harsh present environment of Mars, and particularly the oxidizing agent in the Martian soil, may destroy even this resistant carbonaceous material at most locations unless it is well encapsulated [e.g., *Yen et al.*, 2000].) Graphitic carbon is a strong Raman scatterer (Figure 11) and it is readily and sensitively observed. Graphitic carbon in an ancient South Africa chert was detected by our HoloLab5000 Raman system down to concentrations of <50 ppm [*Wang et al.*, 2001b]. Raman spectra taken by MMRS brassboard on that same sample are shown in Figure 11; definitive spectra were obtained at the <50 ppm concentration level with the MMRS as well, even though the S/N is somewhat lower than that of the HoloLab5000 system.

3.2.2. Understanding Rocks

[39] Raman point counting is the procedure we propose to use to study rocks on Mars [*Haskin et al.*, 1997]. In this procedure, 100 sequential Raman spectra will be taken along a linear traverse on the surface of a rock. Each Raman spectrum obtained will contain the peaks of the minerals excited by the excitation laser beam. Mineral proportions will be estimated from the frequency of appearance of the Raman spectrum of each mineral in the set of spectra. For example, if plagioclase is observed at 40 out of 100 points, then the rock contains ≤40% plagioclase (in some cases, more than one mineral will fall within the excitation volume). To a first approximation, one can claim 40 ± 6% plagioclase (1σ). Such an estimate is usually adequate for rock classification, for which both mineral proportions and mineral grain size are needed. Grain size is inferred to be large if a sequence of points in a scan give spectra of the same mineral and the cation ratio is constant or varies monotonically across the sequence. The proportion of a trace phase cannot be well determined from a 100-point scan; the trace phase can show up more often or less often than its actual proportion in the rock, or it can be missed all together. The frequency with which a trace phase is observed depends on its Raman scattering cross section and on its proportion in the rock or soil, its grain size, and the uniformity of its dispersion. In addition, cation ratios of olivine, pyroxene, and some oxide minerals can be obtained from the spectra, and these provide further information about the origin and alteration of the rocks.

[40] Obtaining this information by Raman point counting requires that a high fraction of the spectra from a point counting traverse have detectable Raman peaks. In our experience, spectra without detectable peaks occur for two general reasons. In one situation, the Raman scatterers yield such a low level of counts that no spectral peak rises above the spectral background noise. This situation most often occurs when the focal plane of the laser beam is offset by several millimeters from the sample surface or when the sample is very dark and there is strong absorption of the laser beam. This problem can often be remedied by increas-

ing the integration time to minutes; this has not been done in the point counting traverses reported here; a fixed counting time was used for all points in a given sample. In the other situation, the spectrum has such a high background that the noise masks the Raman peaks. This usually occurs because the laser has excited a highly fluorescent substance. These spectra are not uninformative, however. Many organic residues encountered in rocks or soils yield high fluorescence, which means that fluorescence is an indicator that such material might be present. Some mineral phases are also fluorescent, and some of these minerals have narrow fluorescent spectral lines that are diagnostic of the particular element (especially the rare earth elements). Inorganic fluorescence from Mn and Fe are common and give broad peaks. The central location of such broadband fluorescent backgrounds, both organic and inorganic in origin, and seen mainly in some carbonates and feldspar, provides information about the origin and history of the host rock.

[41] In most cases, it is more difficult to obtain good spectra from minerals in rocks than from separated, individual mineral grains. Surfaces of rocks are rough, sizes of mineral grains may be small, the laser beam reflects from internal mineral boundaries as well as from the surface of the rocks, and fluorescent phases may be present. These factors all reduce the strength of the Raman signals or increase background. The results from 18 sets of Raman point counting measurements on 9 rock samples of varying degrees of alteration using the MMRS brassboard are summarized in Table 1. Among these rocks, EETA79001,476 is an SNC Martian meteorite of the basaltic shergottite type [*McSween and Jarosewich*, 1983], the Ortenburg basalt is essentially unaltered, the FRB basalt is slightly altered, the AKB basalt is a 1.3 Ga old rock strongly altered by hydrothermal processes [*Brannon*, 1984], the banded calc-silicate is a metamorphic rock, the Missouri red granite is unaltered, Mojave 3256 is a tufa, the MW11-2 chert is a 3.35 Ga chert from South Africa [*Walsh and Lowe*, 1999], and the impactite is from the Manson crater, IA. Of the 433 spectra taken during the Raman point counting measurements on these materials, more than 94% contain interpretable peaks. Based on these spectra, all of the major minerals in all nine rock samples were identified and provided adequate bases to classify the rock types unambiguously. The identification of water- or OH-bearing minerals (e.g., amphibole and epidote in the banded calc-silicate and zeolite in AKB) and of alteration products (e.g., sphene and hematite in FRB) is crucial for determining the environmental histories of these rocks (Figure 12).

[42] Minor and rare mineral phases are likewise important for understanding the origins and alteration of rocks. The discovery and characterization of those phases can depend on their Raman scattering strength and the number of spectra taken during the point counting traverses. Some minor phases are strong scatterers, e.g., phosphate in EETA, hematite in FRB, and calcite in the banded calc-silicate and in the impactite, and were detected from the point counting scans using the MMRS brassboard. Relative to the HoloLab5000, however, the larger spot size of the MMRS excitation laser beam reduces the chance of observing minor phases such as most Fe oxides that are weak scatterers (hematite is an exception). The broader laser beam is more likely to activate major minerals that are stronger scatterers and the signal from the weaker, less abundant scatterers can be overwhelmed by the background of numerous small peaks from the major minerals.

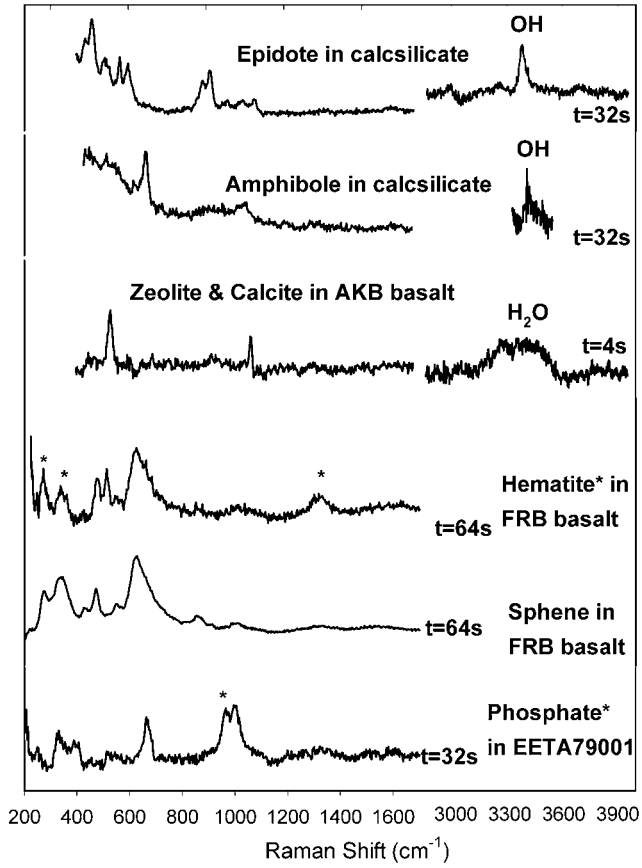

Figure 12. The spectra in this figure were encountered during point count scans on rock samples. The three upper spectra are of water-bearing minerals and they are indicative of the environment in which these minerals formed. The three lower spectra are from minor and trace minerals and also are indicative of the conditions of formation or alteration of their host rocks.

[43] Among the mineral modes of three basaltic rocks derived by Raman point counting (Table 1), only the mode of the Ortenburg basalt is typical for a basalt. The mode of the FRB basalt is recognizably that of a basalt once it is realized that the proportions of sphene and hematite are overestimated. In the case of the minor mineral sphene in the FRB basalt, the overestimation occurs because sphene is a much stronger Raman scatterer than the major minerals, so the laser readily produces its Raman spectrum even when only a trace of sphene falls within the excitation volume. In the case of hematite, the overestimation occurs not only because hematite is a strong scatterer, but also because it is an alteration product that is widely dispersed albeit low in modal abundance. In short, a petrologist must use background knowledge and common sense to interpret the results from a Raman point count. The observation that sphene and hematite are present is important to recognizing the conditions under which the rock formed and was altered. Only a cursory scan across the amygdular fill of the AKB altered basalt was made to observe the calcite and the water-

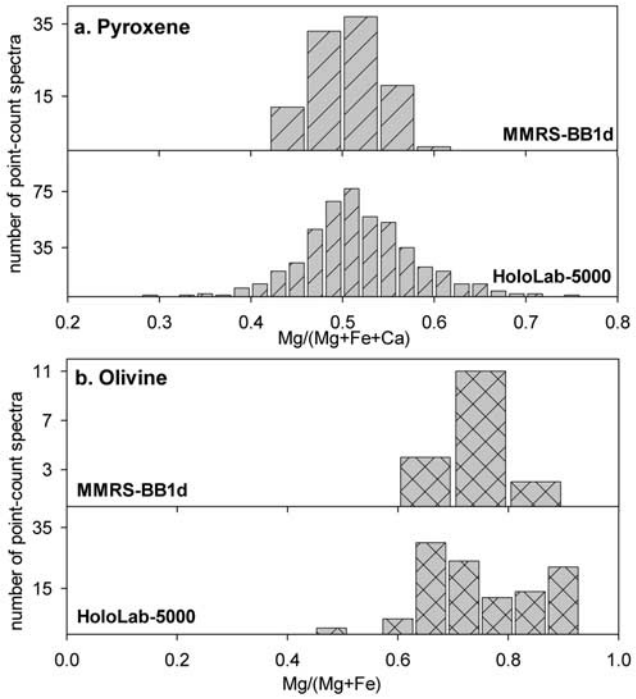

Figure 13. The Raman peak positions of pyroxene and olivine can be used to deduce the ratios of the cations in those minerals [*Wang et al.*, 2001c]. Results are shown for the Mg^{2+} cation ratio (Mg/(Mg + Fe + Ca)) and Mg′ (Mg/(Mg + Fe)) in a chip of the Martian meteorite EETA79001. Note the lower resolution of the MMRS relative to the HoloLab5000, mainly a consequence of the larger diameter of the laser beam of the MMRS, which integrates across wider expanses of compositional zoning. (The flight version of the MMRS will have a much narrower laser beam, which will improve the effective resolution for cation ratio determination.)

bearing zeolite; a detailed Raman study of this rock including the matrix was made earlier [*Wang et al.*, 1999a]. The extent of alteration of AKB is so great that no straightforward mineral mode can be obtained. The original basaltic character of the rock can nonetheless be inferred from its relict pyroxene and plagioclase.

[44] The mode for Martian meteorite EETA79001 leaves out the mineral feldspar (Table 1). Because this rock experienced strong shock pressure during its ejection from Mars, its feldspar was converted to maskelynite, an amorphous material of feldspar composition. Maskelynite has been observed in Martian meteorites using Raman systems [*Cooney et al.*, 1999; *Wang et al.*, 1999b; *Fagan et al.*, 2000]; in fine-grained rocks, glass is more easily observed with a confocal Raman system, in which the Raman signal comes from a much smaller collecting volume than that of our more traditional type of Raman system. Glassy materials have Raman scattering strengths that are much weaker (by ~2 orders of magnitude) than those of crystalline minerals. Although glassy materials can be readily identified when they dominate the spectrum, the Raman peaks of glass can be easily masked by the peaks of the crystalline phases when they are sampled together, which occurs especially when the excitation laser beam is relatively large, as in the present MMRS. Such was the case for 121 of 124 spectra obtained from rock chip 476 of EETA79001; the other three spectra were overwhelmed by a high fluorescent background, and thus no maskelynite could be identified from the spectra of EETA79001 taken by MMRS brassboard. On Mars, feldspar will normally occur as a crystalline phase with a Raman scattering strength similar to that of pyroxene, and thus it can be unambiguously identified. A point count should then provide the correct relative proportions of feldspar and pyroxene (see also the work of *Wang et al.* [1999b] for a discussion of Raman point counting of the Zagami Martian meteorite).

[45] Based on our Raman spectroscopic study of rock chip 476 of Martian meteorite EETA79001 [*Wang et al.*, 1999c, 2000], and in agreement with an earlier petrologic study [*McSween and Jarosewich*, 1983], we observed that this rock cooled rapidly, as indicated by its small grain size (successive spectra were either not of the same mineral or were pyroxene in which the pattern of cation ratios was random and not monotonic, indicating relatively small grains) and the chemical zoning of its pyroxene and olivine mineral grains. In these minerals, Raman peak positions of pyroxene and olivine are dependent on cation ratios of Mg^{2+}, Fe^{2+}, and Ca^{2+} [*Wang et al.*, 2001c; *Guyot et al.*, 1986]. Pyroxene and olivine spectra obtained using the MMRS brassboard on rock chip 476 show variations in peak position over a range of 7 cm^{-1} for pyroxene and 3 cm^{-1} for olivine. These ranges are smaller than those obtained using the HoloLab5000 (18 cm^{-1} for pyroxene and 10 cm^{-1} for olivine) for which the laser beam is much narrower (~6 μm diameter). The narrower range in peak shift is caused by the averaging effect of the larger MMRS laser beam combined with chemical zoning over distances that are short relative to the diameter of the beam. Nevertheless, the distributions of the Mg^{2+} cation molar ratios Mg/(Mg + Fe + Ca) in pyroxene and Mg/(Mg + Fe) in olivine of this rock chip based on measurements done using the MMRS brassboard are consistent with those done on the HoloLab5000 (Figure 13) and with those based on electron microprobe microanalysis [*McSween and Jarosewich*, 1983]. Results are imprecise for the Ca^{2+} cation ratio Ca/(Mg + Fe + Ca) of pyroxene obtained using the MMRS brassboard, for two reasons. One is the error in determining the position of the ~670 cm^{-1} peak because of the lower spectral resolution than is available with a commercial Raman system. The other is the intrinsically weaker correlation between Ca^{2+} cation ratio and Raman peak positions, which occurs because both Ca^{2+} and Fe^{2+} move peaks in the same direction, opposite to that of Mg^{2+} [*Wang et al.*, 2001c].

3.2.3. Tolerance of Adverse Conditions: Rock Surface Roughness and Fine Grain Size

[46] Because no autofocusing mechanism will be used in the MMRS, most Raman spectra in a point counting linear traverse will be collected off-focus. For these measurements, the MMRS must have a high tolerance for rock surface roughness if it is to obtain a high percentage of informative spectra.

[47] We asserted above that the optical design of Raman probe provides a depth-of-sampling field of millimeters. In conjunction with that aspect of the optical design, a high overall level of system light throughput is needed because the Raman signals from off-focus measurements are weaker

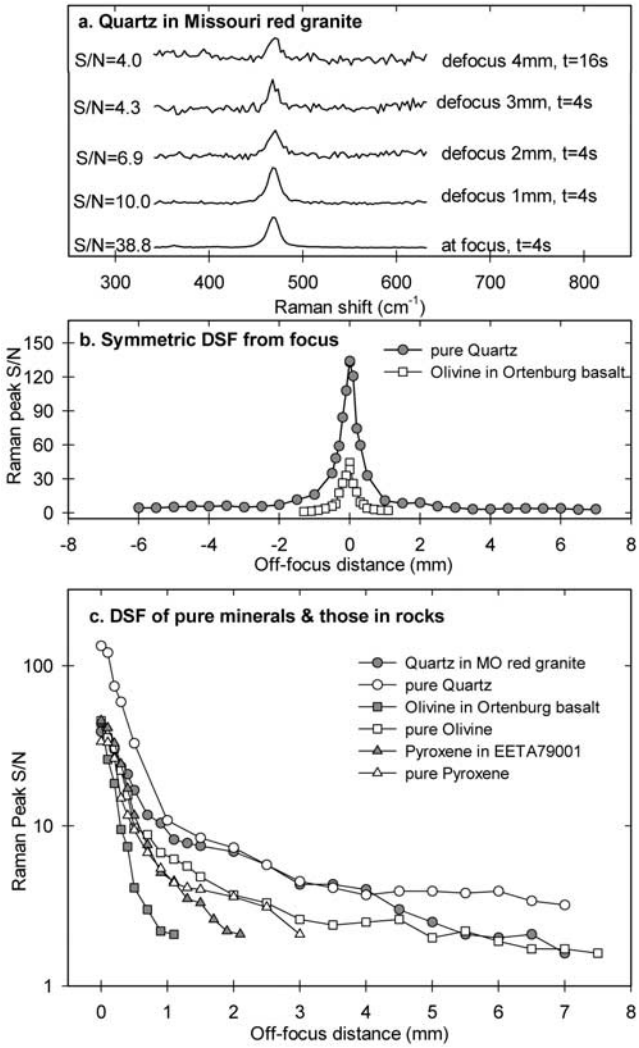

Figure 14. (a) The changes in the spectra that accompany defocusing of the instrument are shown for a favorable situation, quartz in the Missouri red granite. A substantial depth-of-sampling field (DSF) is crucial to compensate for target relief during measurements on rock or soil surfaces as encountered in the field. The spectra are shown in a manner to emphasize the decrease in S/N with increasing distance from the focal plane. (Note the expanded abscissa compared with that of previous figures.) (b) The signal-to-noise ratio for off-focus measurements is symmetric in both directions from focus, i.e., from below or from above the target focal point. This is shown for the single crystal of quartz and for a grain of olivine in the Ortenburg basalt. (c) Signal-to-noise ratios for mineral samples are less sensitive to off-focus distance than those for small mineral grains embedded in rock matrices, as seen here. The single-grain mineral samples are quartz, olivine, and pyroxene; the same as those in Figure 6. The mineral grains in rocks are quartz in the Missouri red granite, olivine in the Ortenburg basalt, and pyroxene in Martian meteorite EETA79001.

than those taken near the focus. This is more of a problem for intrinsically weak Raman scatterers than for strong ones, and the maximum off-focus distance for detecting weak scatterers is thus shorter than that for strong scatterers. An important factor that affects the distance for off-focus detection of a mineral is the nature of the matrix in which it resides and the grain size of that matrix. Off-focus measurements sample a larger area than on-focus measurements, and in a fine-grained material, off-focus measurements can involve Raman signal from several grains rather than just one or two. Thus, if the target is far enough out of focus, only strong scatterers may be detected even when a weak scatterer is within the illuminated volume. If at a particular location a strong scatterer is observed to have a weaker peak intensity than is common at other locations on the target, the location from which that spectrum was obtained may be significantly off focus. Also, if the matrix has a high level of fluorescent emission, or if the matrix is a strong absorber of the excitation laser wavelength, the Raman emission from a particular mineral grain in the matrix could be missed when a large area of matrix gets sampled in an off-focus measurement.

[48] We selected three major rock-forming minerals, quartz (colorless), olivine (moderately dark-colored), and pyroxene (dark-colored), to test the depth-of-sampling field of the MMRS brassboard. The test was made first on single, large mineral grains that contained the entire sampling volume of the Raman probe even at 7 mm off-focus. Then, a set of tests was made on the same minerals but on grains within rock samples: quartz of large grain size (several millimeters) in the Missouri red granite, olivine of smaller grain size (<1 mm) in the almost black Ortenburg basalt, and pyroxene of ~0.15 mm grain size in the gray Martian meteorite EETA79001. Sequential off-focus measurements were made by moving the Raman probe both toward and away from focus in increments of 100–500 μm. The spectra obtained when the probe was moved away from the Missouri red granite are shown in Figure 14a. The quartz spectrum is easily seen at all distances, but the integration times were necessarily longer for the spectra taken farthest from focus. The S/N of the Raman peaks, measured as peak height over the RMS value of the adjacent background, was used to evaluate the detection sensitivity of each mineral when measured off-focus. We observed no obvious difference in rate of change of the S/N in starting the sampling objective below the focal point as opposed to starting it above the focal point (Figure 14b). The S/N of the Raman spectra as a function of the off-focus distance is shown for all six sets of measurements in Figure 14c.

[49] The MMRS brassboard demonstrates an excellent depth-of-sampling field of at least ±7 mm for light colored, strong Raman scatterers such as quartz (carbonates and sulfates would be similar). We found no obvious difference between measurements on individual, isolated pure mineral grains and those on large grains in a light colored rock matrix, except at the farthest off-focus distances, where the large single mineral grains still contained the entire sampling volume but the mineral grain within the rock matrix did not. The depth-of-sampling field of ±2 mm is acceptable for medium strength Raman scatterers such as pyroxene (feldspar and other silicates would be similar) in a light colored rock matrix of fine grain size, as was observed for Martian meteorite EETA79001. Olivine has a fairly large grain size in the Ortenburg basalt and a slightly higher Raman scattering strength than pyroxene (compare the curves in Figure 14c for pure olivine and pure pyroxene).

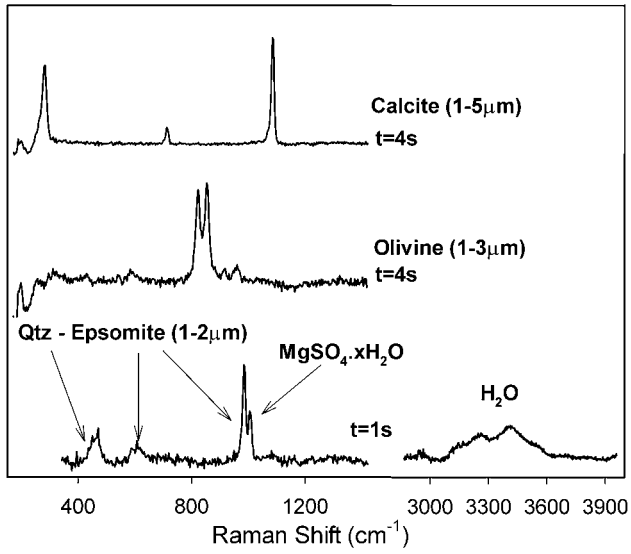

Figure 15. Raman spectra are shown of mineral specimens with a small grain size. The calcite and olivine grains were prepared by grinding larger grains and have grain-size distributions that peak at <1 μm in diameter but reach ~5 and ~3 μm. The epsomite was crystallized from an aqueous solution onto a matrix of fine-grained (~1 μm) quartz. Most of the epsomite grains have diameters in the 1–2 μm range. On standing in the laboratory, some of the epsomite began to lose water of hydration, giving rise to a second peak for both sulfate and water of hydration.

However, the depth-of-sampling field measured by the MMRS brassboard on olivine in Ortenburg basalt is actually shallower than that for pyroxene in EETA79001, only about ±1.2 mm. This appears to be an effect of the stronger competition from absorption in the much darker matrix of the Ortenburg basalt.

[50] Characterizing fine-grained materials on Mars is a challenge for all in situ or remote sensing instruments and that includes the MMRS. The magnitude of the grain size effect depends on the Raman scattering strength of each particular mineral. We have prepared different types of fine-grained samples. In one experiment, crystals of calcite and olivine were separately ground and sieved wet into the following size ranges: >250, 250–150, 150–75, 75–37.5, and <37.5 μm [*Wang*, 1999d]. We took spectra on the smallest of these using MMRS brassboard. In the <37.5 μm size fractions, most of the olivine grains are 1–3 μm in diameter and most of the calcite grains are in the 1–5 μm range [*Kuebler et al.*, 2001]. The measurements were made on heaps of these grains; thus, the effects of surface to volume ratio, porosity, multiple reflections at grain boundaries, and surface roughness are all present. The spectra from these samples are shown in Figure 15. The MMRS brassboard obtained good Raman signals from both samples. We do not observe a spectral pattern change or peak position shift in the Raman spectra of fine grains down to 1 μm, in contrast to some observations using Vis–Near-IR and Mid-IR spectroscopy [*Pieters*, 1983; *Pieters et al.*, 1993a, 1993b; *Lane*, 1999].

[51] Sulfur is abundant in the Martian soil, probably in the form of sulfates [*Clark and Van Hart*, 1981]. Sulfates may be present as evaporite minerals in the duricrust. We produced a simple form of pseudoduricrust by evaporating a solution of $MgSO_4$ onto a matrix of powdered, fine-grained quartz. The sulfate grain size was mostly ≤1 μm [*Kuebler et al.*, 2001]. In raw Raman spectra obtained using the MMRS brassboard (Figure 15), the major Raman peak (982 cm^{-1}) of freshly produced $MgSO_4 \cdot 7H_2O$ and minor peaks at lower Raman shift values were easily observed. The broad peak produced by OH vibrations in the bound H_2O molecules is also visible in the spectrum, but only after flat-field processing. On standing in the laboratory environment for several months, some of the $MgSO_4 \cdot 7H_2O$ was partially dehydrated. The additional peak at 950 cm^{-1} is from that less hydrated form.

4. MMRS Engineering Model

[52] The purpose of this paper has been to demonstrate that we can fabricate a miniaturized Raman spectrometer of near laboratory caliber suitable for use on a planetary surface mission, especially the surface of Mars. The results from the MMRS brassboard have enabled us to fulfill this purpose. One purpose of the MMRS brassboard was to demonstrate feasibility, but another is to progress toward the more sophisticated design that will lead to the actual flight instrument. The results of testing of the brassboard will be used in the design of the engineering model, which is the advanced prototype that will retire the technological risks associated with fabricating a flight instrument and which demonstrates the interfaces with the host rover or lander. These interfaces cannot be fully addressed until they have been specified at the host end, but general aspects of likely interfaces can be anticipated. Here, we list some issues and improvements that the engineering model development will incur. These improvements mainly involve more informed specifications of spectrometer components rather than further technological advances.

[53] A custom grating in the engineering model spectrograph will produce two spectral windows without overlap and will thus stretch the images on the CCD so that the spectral resolution is the desired 7 cm^{-1}. This will increase the wavelength precision of the spectra so that, combined with on-board wavelength calibration using an internal standard, Raman peak positions will be accurate and precise to 1–2 cm^{-1}, which will enable us to constrain more tightly the cation ratios of the minerals.

[54] The throughput of the spectrograph will be improved by a more precise alignment of the input fiber with the slit and by optimizing the lenses and coatings for transmission of wavelengths corresponding to Raman shifts from the green 532 nm wavelength. These changes are expected approximately to double the throughput of the spectrograph and thus the detection sensitivity.

[55] The filters that remove the reflected laser light and the Rayleigh-scattered light from the Raman signal will have a steeper slope between cutoff of the laser wavelength and transmittance of Raman-scattered photons. This will significantly increase the sensitivity of the instrument for Raman shifts in the 180–350 cm^{-1} range.

[56] From our experience with the MMRS brassboard, we are learning how to specify the software commands for autocontrol of integration time at each target point, in order to avoid saturation from photoluminescence, increase the

Raman S/N relative to photoluminescence, and to ensure adequate integration for weak Raman scatterers.

[57] Now that the efficacy of a small excitation laser of green wavelength has been proven, a specific laser and its configuration will be selected. This selection will improve the optical design of the probe. A narrower laser beam will be sent to the target, still retaining the effective depth-of-sampling field of several millimeters. The laser will also be operable in a low-power mode for detection of heat-sensitive minerals and in a higher-power mode for more robust minerals.

[58] In summary, the present brassboard of MMRS reaches ~20% of the detection sensitivity of our state-of-the-art laboratory Raman system with slightly poorer spectral resolution. The above improvements will at least double the sensitivity and improve the spectral resolution.

[59] **Acknowledgments.** This work was supported by NASA grants NAG5-7140 and NAG5-10703. We gratefully acknowledge contributions to the development of this instrument provided by the following individuals and their organizations: Jose Apodaca, Joel Johnson, Gordon Mon, Olga Shchedrin, and Jim Shea of the Pasadena Office of the Swales Aerospace Corporation for optical, mechanical, and thermal design; James Arns of Kaiser Optical Systems, Inc. for grating design; Boris Shnapir of Barr Associates for filter design; and Mark Wadsworth and Tom Elliot of the Jet Propulsion Laboratory for CCD detector selection and testing, with component assistance from the Phillips Corporation. Important individual contributions came from Matt Novak, Siamak Forouhar, Gindi French, Curtis Keedy, Joe Mansour, John Johnston, and Kai Zhu of the Jet Propulsion Laboratory.

References

Arns, J. A., Holographic transmission grating improve spectroscopy and ultrafast laser performance, *SPIE Proc.*, *2404*, 174–181, 1995.

Battey, D. E., J. B. Slater, R. Wludka, H. Owen, D. M. Pelletier, and M. D. Morris, Axial transmissive f/1.8 imaging Raman spectrograph with volume-phase holographic filter and grating, *Appl. Spectrosc.*, *47*, 1913–1919, 1993.

Bell, J. F., III, Iron, sulfate, carbonate, and hydrated minerals on Mars, in *Mineral Spectroscopy: A Tribute to Roger G. Burns, Geochem. Soc. Spec. Publ.*, vol. 5, edited by M. D. Dyar et al., pp. 359–380, Geochemical Soc., Houston, Texas, 1996.

Bell, J. F., et al., Minerologic and compositional properties of Martian soil and dust: Results from Mars Pathfinder, *J. Geophys. Res.*, *105*, 1721–1755, 2000.

Brannon, J. C., Geochemistry of successive lava flows of the Keweenawan North Shore Volcanic Group, Ph.D. dissertation, Washington Univ., St. Louis, MO, 1984.

Christensen, P. R., et al., Mars Global Surveyor Thermal Emission Spectrometer experiment: Investigation description and surface science results, *J. Geophys. Res.*, *106*, 23,823–23,871, 2001.

Clark, B. C., and D. C. Van Hart, The salt of Mars, *Icarus*, *45*, 370–378, 1981.

Cooney, T. F., H. T. Skinner, and S. M. Angel, Comparative study of some fiber-optic remote Raman probe designs, part 1, Models for liquids and transparent solids, *Appl. Spectrosc.*, *50*, 836–848, 1996.

Cooney, T. F., H. T. Skinner, and S. M. Angel, Comparative study of some fiber-optic remote Raman probe designs, part 2, Tests of single-fiber, lensed, and flat- and bevel-tip multi-fiber probes, *Appl. Spectrosc.*, *50*, 849–860, 1996.

Cooney, T. F., E. R. D. Scott, A. N. Krot, S. K. Sharma, and A. Yamaguchi, Vibrational spectroscopic study of minerals in the Martian meteorite ALH84001, *Am. Mineral.*, *84*, 1569–1576, 1999.

Dhamelincourt, P., and J. Barbillat, Raman microscopy, in *Handbook of Microscopy: Methods I*, Chap. 5, edited by S. Amelinckx et al., p. 54, John Wiley, New York, 1997.

Dickensheets, D., D. D. Wynn-Williams, H. G. M. Edwards, C. Schoen, C. Crowder, and E. M. Newton, A novel miniature confocal microscope/Raman spectrometer system for biomolecular analysis on future Mars missions after Antarctic trials, *J. Raman Spectrosc.*, *31*, 633–635, 2000.

Edwards, H. G. M., D. W. Farwell, M. M. Grady, D. D. Wynn-Williams, and I. P. Wright, Comparative Raman spectroscopy of a Martian meteorite and Antarctic lithic analogues, *Planet. Space Sci.*, *47*, 353–362, 1999.

Exobiology Program Office, NASA HQ, An exobiological strategy for Mars exploration, *NASA Spec. Pap. SP, 530*, 1995.

Fagan, T. J., E. R. D. Scott, K. Keil, T. F. Cooney, and S. K. Sharma, Formation of feldspathic, metallic, and enstatitic melts by shock in enstatite chondrite Reckling Peak A80259, *Meteorit. Planet. Sci.*, *35*, 319–329, 2000.

Fonti, S., A. Jurewicz, A. Blanco, M. I. Blecka, and V. Orofino, Presence and detection of carbonates on the Martian surface, *J. Geophys. Res.*, *106*, 27,815–27,822, 2001.

Guyot, F., H. Boyer, M. Madon, B. Velde, and J. P. Poirier, Comparison of the Raman microprobe spectra of $(Mg,Fe)_2SiO_4$ and Mg_2GeO_4 with olivine and spinel structures, *Phys. Chem. Miner.*, *13*, 91–95, 1986.

Hargraves, R. B., J. M. Knudsen, P. Bertelsen, W. Goetz, H. P. Gunnlauggsson, S. F. Hviid, M. B. Madsen, and M. Olsen, Magnetic enhancement on the surface of Mars?, *J. Geophys. Res.*, *105*, 1819–1827, 2000.

Haskin, L. A., A. Wang, K. M. Rockow, B. L. Jolliff, R. L. Korotev, and K. M. Viskupic, Raman spectroscopy for mineral identification and quantification for in-situ planetary surface analysis: A point count method, *J. Geophys. Res.*, *102*, 19,293–19,306, 1997.

Kargel, J. S., K. L. Tanaka, V. R. Baker, G. Komatsu, and D. R. MacAyeal, Formation and dissociation of clathrate hydrates on Mars: Polar caps, northern plains, and highlands, *Lunar Planet. Sci.*, *XXXI*, abstract 1891, 2000.

Klingelhöfer, G., The miniaturized spectrometer MIMOS II: The 2001 and 2003 US Mars missions and terrestrial applications in materials science and industry, in *Mossbauer Spectroscopy in Materials Sciences*, edited by M. Miglierini and D. Petridis, Kluwer Acad., Norwell, Mass., 1999.

Komatsu, G., J. S. Kargel, V. R. Baker, R. G. Strom, G. G. Ori, C. Modangini, and K. L. Tanaka, A chaotic terrain formation hypothesis: Explosive outgas and outflow by dissociation of clathrate on Mars, *Lunar Planet. Sci.*, *XXXI*, abstract 1434, 2000.

Kuebler, K. E., A. Wang, K. Abbott, and L. A. Haskin, Can we detect carbonate and sulfate minerals on the surface of Mars by Raman spectroscopy?, *Lunar Planet. Sci.*, *XXXII*, abstract 1889, 2001.

Kudryavtsev, A. B., J. W. Schopf, D. G. Agresti, and T. J. Wdowiak, In situ laser imagery of Precambrian microscopic fossils, *Proc. Natl. Acad. Sci.*, *98*, 823–826, 2001.

Lane, M. D., Midinfrared optical constants of calcite and their relationship to particle size effects in thermal emission spectra of granular calcite, *J. Geophys. Res.*, *104*, 14,099–14,108, 1999.

Long, D. A., *Raman Spectroscopy*, pp. 2–5, McGraw-Hill, New York, 1977.

Longhi, J., Low-temperature phase relations in the CO_2–H_2O system with application to Mars, *Lunar Planet. Sci.*, *XXXI*, abstract 1518, 2000.

Longhi, J., Clahtrate and ice stability in a porous Martian regolith, *Lunar Planet. Sci.*, *XXXII*, abstract 1955, 2001.

Madsen, M. B., S. F. Hviid, H. P. Gunnlauggsson, J. M. Knudsen, W. Goetz, C. T. Pedersen, A. R. Dinesen, C. T. Mogensen, and M. Olsen, The magnetic properties experiments on Mars Pathfinder, *J. Geophys. Res.*, *104*, 8761–8779, 1999.

McSween, H. Y., Jr., and E. Jarosewich, Petrogenesis of the Elephant Moraine A79001 meteorite: Multiple magma pulses on the shergottite parent body, *Geochim. Cosmochim. Acta*, *47*, 1501–1513, 1983.

Morris, R. V., et al., Mineralogy, composition, and alteration of Mars Pathfinder rocks and soils: Evidence from multispectral, elemental, and magnetic data on terrestrial analogue, SNC meteorite, and Pathfinder samples, *J. Geophys. Res.*, *105*, 1757–1817, 2000.

Morris, R. V., D. C. Golden, D. W. Ming, T. D. Shelfer, L. C. Jorgensen, J. F. Bell III, T. G. Graff, and S. A. Mertzman, Phyllosilicate-poor palagonitic dust from Mauna Kea Volcano (Hawaii): A mineralogical analogue for magnetic Martian dust, *J. Geophys. Res.*, *106*, 5057–5083, 2001.

Pieters, C. M., Strength of mineralogical absorption features in the transmitted component of reflection: First results from RELAB, *J. Geophys. Res.*, *88*, 9534–9544, 1983.

Pieters, C. M., E. M. Fischer, O. Rode, and A. Basu, Optical effects of space weathering: The role of the finest fraction, *J. Geophys. Res.*, *98*, 20,817–20,824, 1993a.

Pieters, C. M., J. F. Mustard, S. F. Pratt, J. M. Sunshine, and A. Hoppin, Visible infrared properties of controlled laboratory soils, *Proc. Lunar Planet. Sci. Conf.*, *XXIV*, 1147–1148, 1993b.

Rieder, R., H. Wänke, T. Economou, and A. Turkevich, Determination of the chemical composition of Martian soils and rocks: The alpha proton X-ray spectrometer, *J. Geophys. Res.*, *102*, 4027–4044, 1997.

Schoen, C. L., T. F. Cooney, S. K. Sharma, and D. M. Carey, Long fiber-optic remote Raman probe for detection and identification of weak scatterers, *Appl. Opt.*, *31*, 7707–7715, 1992.

Sharma, S. K., C. L. Schoen, and T. F. Cooney, Fiber-optic remote Raman probe design for use in monitoring processes in a high-temperature oven, *Appl. Spectrosc.*, *47*, 377–379, 1993.

Squyres, S. W., et al., The Mars 2001 Athena Precursor Experiment (APEX), *Lunar Planet. Sci.*, *XXX*, abstract 1672, 1999.

Soderblom, L. A., The composition and mineralogy of the Martian surface from spectroscopic observations: 0.3 μm to 50 μm, in *Mars*, Chapter 17, edited by H. H. Kieffer et al., pp. 557–593, 1498 pp., Univ. of Ariz. Press, Tucson, 1992.

Sum, A. K., R. C. Burruss, and E. D. Sloan, Jr., Measurement of clathrates via Raman spectroscopy, *J. Phys. Chem.*, *B101*, 7371–7377, 1997.

Walsh, M. M., and D. R. Lowe, Modes of accumulation of carbonaceous matter in the early Archean: A petrographic and geochemical study of the carbonaceous cherts of the Swaziland Supergroup, in *Geologic Evolution of the Barberton Greenstone Belt, South Africa, Spec. Pap. Geol. Soc. Am.*, vol. 32, edited by D. R. Lowe and G. R. Byerly, pp. 115–132, Geol. Soc. of Am., Boulder, 1999.

Wang, A., Some grain size effects on Raman scattering intensity for in situ measurements on rocks and soils: Experimental tests and modeling, *Lunar Planet. Sci.*, *XXX*, abstract 1644, 1999.

Wang, A., and R. B. Valentine, Seeking and identifying phyllosilicates on Mars: A simulation study, *Lunar Planet. Sci.* [CD-ROM], *XXXIII*, abstract 1370, 2002.

Wang, A., J. Han, L. Guo, J. Yu, and P. Zeng, A database of standard Raman spectra of mineral and related inorganic crystals, *Appl. Spectrosc.*, *48*, 959–968, 1994.

Wang, A., B. L. Jolliff, and L. A. Haskin, Raman spectroscopy as a method for mineral identification on lunar robotic exploration missions, *J. Geophys. Res.*, *100*, 21,189–21,199, 1995.

Wang, A., L. A. Haskin, and E. Cortez, A Raman spectroscopic sensor for in situ mineral characterization on planetary surface, *Appl. Spectrosc.*, *52*, 477–487, 1998a.

Wang, A., L. A. Haskin, and B. L. Jolliff, Characterization of mineral products of oxidation and hydration by laser Raman spectroscopy: Implications for in situ petrologic investigation on the surface of Mars, *Lunar Planet. Sci.*, *XXVIII*, abstract 1819, 1998b.

Wang, A., B. L. Jolliff, and L. A. Haskin, Raman spectroscopic characterization of a highly weathered basalt: Igneous mineralogy, alteration products, and a micro-organism, *J. Geophys. Res.*, *104*, 27,067–27,077, 1999a.

Wang, A., B. L. Jolliff, and L. A. Haskin, Raman spectroscopic characterization of a Martian SNC meteorite Zagami, *J. Geophys. Res.*, *104*, 8509–8519, 1999b.

Wang, A., B. L. Jolliff, L. A. Haskin, and K. E. Kuebler, Raman spectral features of pyroxene: Application to Martian meteorites Zagami & EETA79001, *Lunar Planet. Sci.*, *XXX*, abstract 1666, 1999c.

Wang, A., K. E. Kuebler, B. L. Jolliff, and L. A. Haskin, Mineral features of EETA79001 Martian meteorite revealed by point-counting Raman measurements as anticipated for in-situ exploration on planetary surfaces, *Lunar Planet. Sci.*, *XXXI*, abstract 1887, 2000.

Wang, A., K. E. Kuebler, and B. L. Jolliff, Raman spectroscopy of opaque minerals and applications to EETA79001 Martian meteorite, *Lunar Planet. Sci.*, *XXXII*, abstract 1615, 2001a.

Wang, A., L. A. Haskin, K. E. Kuebler, B. L. Jolliff, and M. M. Walsh, Raman spectroscopic detection of graphitic carbon of biogenic parentage in an ancient South African chert, *Lunar Planet. Sci.*, *XXXII*, abstract 1432, 2001b.

Wang, A., B. L. Jolliff, L. A. Haskin, K. E. Kuebler, and K. M. Viskupic, Characterization and comparison of structural and compositional features of planetary quadrilateral pyroxenes by Raman spectroscopy, *Am. Mineral.*, *86*, 790–806, 2001c.

Wang, A., J. Freeman, and K. E. Kuebler, Raman spectroscopic characterization of phyllosilicates, *Lunar Planet. Sci.*, *XXXIII*, abstract 1374, 2002.

Wopenka, B., and J. D. Pasteris, Structural characterization of kerogens to granulite-facies graphite: Applicability of Raman microprobe spectroscopy, *Am. Mineral.*, *78*, 533–557, 1993.

Wynn-Williams, D. D., and H. G. M. Edwards, Proximal analysis of regolith habitats and protective biomolecules in situ by laser Raman spectroscopy: Overview of terrestrial Antarctic habitats and Mars analogs, *Icarus*, *144*, 486–503, 2000.

Yen, A. S., S. S. Kim, M. H. Hecht, M. S. Frant, and B. Murray, Evidence that reactivity of the Martian soil is due to superoxide ions, *Nature*, *289*, 1909–1912, 2000.

L. A. Haskin and A. Wang, Department of Earth and Planetary Sciences and McDonnell Center for the Space Sciences, Washington University, One Brookings Drive, St. Louis, MO 63130, USA. (alianw@levee.wustl.edu)

L. E. Hovland, A. L. Lane, K. S. Manatt, N. Raouf, and R. J. Wilson, Jet Propulsion Laboratory, 4800 Oak Grove Drive, Pasadena, CA 91109, USA.

C. D. Smith, Swales Aerospace Corp., 404 N. Halstead Street, Pasadena, CA 91107, USA.

S. W. Squyres, Center for Radiophysics and Space Physics, Cornell University, Ithaca, NY 14853, USA.

T. J. Wdowiak, Department of Physics, University of Alabama at Birmingham, Birmingham, AL 35294-1170, USA.